FUNDAMENTAL INVESTIGATIONS INTO TWO OXYGEN-SENSITIVE METALLOENZYMES FROM THE HYPERTHERMOPHILIC ANAEROBE *PYROCOCCUS FURIOSUS*

by

BRET DONALD DILLARD

(Under the Direction of MICHAEL W. W. ADAMS)

ABSTRACT

The objective of this research was to gain a more complete understanding of the enzymatic activities of two oxygen-sensitive enzymes from *Pyrococcus furiosus*. When working with these enzymes from this obligate anaerobe, it is necessary that all manipulations be carried out in an anaerobic environment in order to maintain the stability of both the metal cofactors and the proteins.

The first aim was to show that proline dehydrogenase 1 (PDH1) contains an iron-sulfur cluster and to determine its role in catalysis. The cluster was not evident in the published crystal structure reported by others due to the fact that the protein was prepared aerobically. Using anaerobically purified PDH1, it was shown in this work by electron paramagnetic resonance and inductively coupled plasma spectroscopic analyses that it contains a [2Fe-2S] cluster and that it is reduced by proline, the natural substrate. It is also shown that the cluster transfers electrons to an artificial electron acceptor, resorufin, only when the enzyme is maintained in an anoxic environment. In addition, when the cluster is present in the enzyme, its affinity for proline increases by two orders of magnitude.

The second aim of this research was to determine the structure of the iron-containing enzyme rubrerythrin in its native form in both the reduced and oxidized states. The enzyme precipitates when exposed to oxygen or to an excess of its substrate, hydrogen peroxide. In order to maintain its enzymatic activity, the enzyme must be maintained in an anaerobic environment. For crystallization trials, two approaches were merged to make an efficient tool for screening and optimizing the crystallization in an anaerobic environment. The crystal structure of rubrerythrin was shown to contain three iron atoms per monomer and its unique feature of domain swapping was confirmed. The structure of the oxidized form gave great insights into both the catalytic mechanism and the cause of the precipitation of the enzyme upon oxidation.

INDEX WORDS: *Pyrococcus furiosus*, hyperthermophilic archaea, proline dehydrogenase, rubrerythrin, X-ray crystallography

FUNDAMENTAL INVESTIGATIONS INTO TWO OXYGEN SENSITIVE METALLOPROTEINS FROM THE OBLIGATE ANAEROBE *PYROCOCCUS FURIOSUS*

by

BRET DONALD DILLARD

B.S., University of Georgia, 2003

A Dissertation Submitted to the Graduate Faculty of The University of Georgia in Partial Fulfillment of the Requirements for the Degree

DOCTOR OF PHILOSOPHY

ATHENS, GEORGIA

FUNDAMENTAL INVESTIGATIONS INTO TWO OXYGEN SENSITIVE

METALLOPROTEINS FROM THE OBLIGATE ANAEROBE *PYROCOCCUS FURIOSUS*

by

BRET DONALD DILLARD

Major Professor: M. W. W. ADAMS

Committee: W. N. LANZILOTTA
J. ROSE
B. C. WANG

Electronic Version Approved:

Maureen Grasso
Dean of the Graduate School
The University of Georgia
July 2010

DEDICATION

This dissertation is dedicated to my wife, Allison Appleton Dillard. When we first met I was an underachieving manager of a local restaurant in Athens, Ga. I knew when I fell in love with her that it would take more than being a glorified cook to keep her around, not that she wanted it, but because she deserves it. It was her love for me that has led to the work described herein. She has shown me many great things in life and in love and has given me my most beautiful creation, Elizabeth Gray Dillard. Without her unwavering support, be it financial, inspirational, or emotional, none of this would have been possible. There is no other person in the world that can come close to deserving this dedication more than her.

ACKNOWLEDGEMENTS

I must first acknowledge Dr. Michael W. W. Adams for his guidance, humor, ribbing, intelligent conversation, and caring personality during the execution of the work described in this dissertation. He is truly a wonderful mentor and a very incredible man. His only concern during this entire period of my life was to help me become a better scientist and to be able to carry that out into the real world. I am truly thankful for that.

Secondly, I would like to thank my committee members who have helped to shape and mold not only the work described here, but also my views on how science should be carried out. Dr. William Lanzilotta was the first to get me seriously involved in biochemistry when I was finishing my undergraduate degree and he taught me the beginnings of my crystallographic love/hate affair; not to mention his indispensable help in solving the last structure described in this dissertation. Dr. Bi-Cheng Wang then accepted me as an entering graduate student and helped me to understand more the fundamentals of crystallographic analysis and how to pay attention to detail when looking at any problem. Dr. John Rose, whose extensive knowledge of the programs that manipulate crystallographic data was essential in carrying out the latter two crystal structures described in this thesis and others deposited in the protein data bank. Without these committee members I am scared to think of where I would be had I chosen others.

I would also like to thank Dr. Peter Horanyi for his endless encouragement and willingness to discuss whatever thing it was I was trying to polish.

Others involved in my professional development and the production of this dissertation that should be mentioned are Dr. Gerritt (Gerti) Schut, whose discussions about the possible

roles of PDH1 helped tremendously. Dr. Frank Sugar, for his friendship and guidance in my early years as a graduate student. Dr. Francis Jenney, who also helped with many great discussions. All of these gentlemen have aided the growth of my knowledge about biochemistry in general and specifically my ability to manipulate proteins to get a story out of them.

There are those that helped me in the form of friendship, although they are scientists as well, they were not involved directly in the outcome of this dissertation and they are, in no particular order: Quentin Florence, Chris Hopkins, Stephanie Bridger, Sonya Clarkson, Heather Strachan, Jon Demick, Stephen Porter, and all of the members of the Adams lab.

I would also like to acknowledge my father Dr. James D. Dillard and my step mother Kimberly Dillard as well as my brothers, Ryan and Casey. I would like to acknowledge my parents in-law Dr. Brown Gray Appleton and Linda Appleton as well. It is so nice to have a set of people that support and love you no matter what. It is also nice to have people that don't ask, "When are you gonna finish?" with an attitude that can only be misconstrued by someone doing graduate work.

Lastly, I would like to acknowledge God in all that He has done for me and the luck and help that He has blessed me with over my entire life.

TABLE OF CONTENTS

Page

LIST OF TABLES

Page

LIST OF FIGURES

Page

CHAPTER 1

Introduction and Literature Review

Archaea were first recognized as the third domain of life after Carl Woese constructed a new tree of life based on 16S ribosomal RNA sequences (*1*). The tree of life that was constructed contains three major groups or branches that are termed domains. These three domains are eukarya, bacteria, and archaea where each domain is derived from one common ancestor (Figure1.1) (*1, 2*). Archaea and bacteria are similar in that they are single-celled prokaryotes but differ in their transcription and translation machinery. In addition, archaea have cell walls that lack peptidoglycan and membranes that contain ether linkages rather than ester bonds.

Initially it was the extreme environments in which archaea had been found that suggested they were a diverse group of organisms, but more recently they have been discovered in more moderate environments such as soils and the open ocean (*3*). However, originally archaea were found in environments that are high in salinity, acidity, as well as environments of high and low temperature and it is their ability to thrive in such conditions that has given many of them the moniker, extremophile (*4*). The archaeal domain includes a total of four phyla, which are the Crenarchaeota, Euryarchaeota, Korarchaeota, and most recently discovered, the Nanoarchaeaota (*5, 6*). The Crenarchaeota and Euryarchaeota have been studied extensively, while Korarchaeota exist only due to the discovery of their 16S rRNA and the Nanoarchaeota live as symbionts. A majority of the Crenarchaeota are hyperthermophiles meaning that they grow optimally at temperatures above 80°C while the Euryarchaeota have a greater diversity of growth optima; there are many examples of mesophiles in this phylum (*5*).

Hyperthermophilic organisms are characterized as those that have an optimal growth temperature above 80°C (*7*). To date, the highest growth temperature achieved by an archaeal hyperthermophile is that of *Methanopyrus kandleri* which grows at 122°C (*8*). Of the hyperthermophiles, all are archaea with two exceptions, *Aquifex* and *Thermotoga,* which belong to the domain bacteria. The environments from which these organisms have been isolated vary greatly with the first distinction being terrestrial or marine. Terrestrial environments include sofataric fields, mud holes, and hot springs, which are located near volcanoes. The marine environments from which these organisms are isolated are varied more greatly in that they can be shallow and near the coast (Vulcano Island, Italy) or near deep-sea hydrothermal vents. Once again this environment is associated with volcanic activity. The most recognizable feature of the deep sea hydrothermal vent is where they get the common name "black smoker". The black smoke is composed of precipitated metal sulfides (*9*). The temperature of the water varies greatly around these hydrothermal vents from close to 400°C to 2°C and this allows for different organisms to fill specific niches that create a very diverse community (*10*). There are also many distinctions among the organisms in how they consume energy. The hyperthermophilic group includes organisms that are denitrifiers, sulfur reducers, sulfate reducers, methanogens and some that reduce oxygen (*7*). Many hyperthermophiles are obligate anaerobic heterotrophs in that they consume peptides or carbohydrates as a carbon source, and many of these utilize peptides in a sulfur dependent manner. *Pyrococcus furiosus* is an example of an anaerobic hyperthermophilic archaeon that degrades peptides in a sulfur-dependent manner and can also utilize carbohydrates independent of the presence of sulfur (Figure 1.2). In the following chapter it will be demonstrated that an enzyme from *P. furiosus* involved in the consumption of peptides contains an iron-sulfur cluster that is necessary in the transfer of electrons from the substrate proline.

Another feature of this obligate anaerobe investigated in chapters 3 and 4 is the enzyme rubrerythrin, which is involved in the oxygen detoxification pathway of this organism. The next sections of this chapter will describe separately what is known about the two pathways.

Metabolism of Peptides by *Pyrococcus furiosus*

P. furiosus can grow on peptides only when elemental sulfur is available (*11*). The growth rate of *P. furiosus* is most rapid when the organism is fermenting peptides in the presence of sulfur as opposed to growth on maltose in the presence or absence of sulfur (*11*). When the organism is utilizing peptides as a carbon source the first step is convert the peptides to individual amino acids by peptidases. Peptidases that have been characterized from this organism include prolidase, lysine-specific aminopeptidase, cobalt-activated carboxypeptidase and pyrollidone carboxypeptidase (*12-14*). Once the peptides are converted to individual amino acids they are metabolized further to 2-keto acids by specific aminotransferases. *P. furiosus* contains four distinct 2-keto acid oxidoreductases that convert the products from the aminotransferases into their respective acyl CoA moieties. These four oxidoreductases are termed (1) indolepyruvate oxidoreductase (IOR) which acts on aromatic 2-keto acids, (2) isovalerate oxidoreductase (VOR) which acts on branched chain 2-keto acids, (3) pyruvate oxidoreductase (POR) which acts on pyruvate, and (4) ketoglutarate oxidoreductase (KGOR) which acts on 2-ketoglutarate (*15-19*). An alternative to this pathway, dependent upon the metabolism of the organism, is that the 2-keto acids can be decarboxylated to form aldehydes by one of the previously mentioned oxidoreductases in a ferredoxin independent manner such that aldehyde oxidoreductase could convert them into a useful molecule for the cell (*20*). Once the acyl CoA derivatives are generated by the respective oxidoreductases, which also produce reduced ferredoxin, they are acted on by two distinct enzymes termed acyl CoA synthetase 1 and

2 (ACS1 and ACS2) (*21*). These enzymes convert the acyl CoA derivatives, with the exception of succinyl-CoA generated by the activity of KGOR, into organic acids and couple the reaction to the generation of ATP (*21*). There is an overlap in the substrate specificity in that the two enzymes both work on the products from the reactions of POR and VOR but only ACS2 can convert the products generated by the reaction from IOR. An interesting note is that neither enzyme has activity towards succinyl CoA generated by KGOR, which could possibly be used in biosynthesis or in an anaerobic form of the citric acid cycle. *P. furiosus* has been shown to contain at least two of the enzymes contained in the oxidative citric acid cycle such as fumarase (PF1754-1755) and aconitase (PF0201) which is unexpected for an anaerobe (*22*). In chapter two, the activity of proline dehydrogenase will be discussed. This enzyme is responsible for the conversion of proline to pyrroline-5-carboxylic acid. It is interesting to note that without this enzyme the previously described pathway could not be utilized, as the oxidative deamination step could not occur as the nitrogen is involved in a secondary amine bond. Proline dehydrogenase breaks the cyclic nature of this amino acid by the two-electron oxidation of its substrate, which is then followed by non-enzymatic hydrolysis to L-glutamate 5-semialdehyde. Once this occurs, L-glutamate 5-semialdehyde could be converted to glutamate by another two-electron oxidation by either L-glutamate 5-semialdehyde dehydrogenase or pyrroline-5-carboxylate dehydrogenase. At this point glutamate could be used in either of two reactions. The first is by entering the glutamate dehydrogenase cycle, which generates NADPH and ammonia, or it is converted to 2-ketoglutarate and follows the pathway through KGOR to generate ATP and reduced ferredoxin depending on the energy metabolism of the cell at that point. The entire pathway from peptides to organic acids is outlined in Figure 1.3.

Oxidative stress response in *P. furiosus*

The formation of reactive oxygen species (ROS) occurs by the incomplete reduction of oxygen to water. Such species include superoxide, hydrogen peroxide, and the hydroxyl radical (*23*, *24*). Oxygen can freely cross cellular membranes and accept electrons in a univalent manner to generate these intermediates (*25*). The single electron transfer occurs by ROS molecules entering active sites of redox enzymes and accepting electrons from a lower potential redox sites, flavin-containing enzymes are thought to be a primary source (*26*). The standard reduction potentials of the different species of reactive oxygen intermediates are as follows (*27*):

$$O_2 \xrightarrow{-0.16V} O_2^{\cdot -} \xrightarrow{+0.94V} H_2O_2 \xrightarrow{+0.38V} {\cdot}OH + H_2O \xrightarrow{+2.33V} H_2O$$

The rate of formation of the superoxide radical and of hydrogen peroxide have been estimated to be 15 µM/s and 5 µM/s inside the cell of *Escherichia coli*, respectively (*28*). Hydrogen peroxide can also be formed by reduced metals and different sulfur species that originate in anaerobic environments and come into contact with oxygen-rich water (*27*). This non-charged molecule can then also freely diffuse across the cellular membrane. Once ROS molecules are in the cell they can cause massive damage if not removed immediately, including damage to DNA, disulfide and iron-sulfur cluster containing enzymes, and membrane lipids. While the damage to iron-sulfur cluster containing enzymes can come from the direct interaction of these molecules where they oxidize the cluster and release iron, many of the consequences to the cell are of indirect interactions of these molecules generating hydroxyl radicals that directly damage DNA (*29*). Hydrogen peroxide is a part of the Fenton reactions that create oxidized species of iron, which can then generate hydroxyl radicals according to equations 1 and 2 (*30*):

$$Fe^{2+} + H_2O_2 \longrightarrow FeO^{2+} + H_2O \quad (1)$$

$$FeO^{2+} + H^+ \longrightarrow Fe^{3+} + {\cdot}OH \quad (2)$$

It is currently thought that free hydroxyl radicals are not responsible for DNA damage directly but that it is the local iron-oxo species arising from the chelation of iron by DNA that actually cause the damage (*31*). It is possible that iron associated with proteins and lipids could undergo the same reaction but there is no evidence either proving or disproving this idea.

It has been shown that these oxygen reactive intermediates can freely cross the cell membrane and cause widespread damage, so it is very important that organisms have a rapid defense system for this problem. Early life evolved in an anaerobic environment and therefore these defenses were unnecessary but upon the development of photosystem 2, oxygen levels in the atmosphere began to slowly rise and thus countermeasures were necessary. The next section will detail how aerobic and anaerobic organisms deal with these problems.

The one electron reduction of oxygen leads to superoxide which aerobic organisms have developed a defense against in the form of superoxide dismutase (SOD), which converts superoxide to hydrogen peroxide. Multiple forms of this enzyme have been discovered in *E. coli* where there are two cytoplasmic forms as well as a periplasmic form. The two forms in the cytoplasm contain either iron or manganese as a cofactor while the periplasmic form uses a copper/zinc cofactor (*32*). These enzymes are expressed at a level to maintain the superoxide concentration inside the cell low enough to where it will inactivate sensitive proteins only minimally and then repair processes take over. Once hydrogen peroxide has been generated by SOD, peroxidases and catalases convert it to water and oxygen. Thus the complete removal of reactive oxygen species in aerobes is as follows in equations 3-5:

$2O_2^- + 2H^+ \rightarrow O_2 + H_2O_2$ SOD (3)

$2H_2O_2 \rightarrow O_2 + 2H_2O$ Catalase (4)

$RH_2 + H_2O_2 \rightarrow R + 2H_2O$ Peroxidase (5)

These organisms also have inducible responses to reactive oxygen intermediates for when they encounter an environment in which these molecules can overwhelm the basal level of defense. These systems have been well characterized and are as follows; SoxR and SoxS as responses to superoxide and OxyR and PerR as responses to excess hydrogen peroxide (*33-36*). SoxR is a sensor protein of superoxide that induces the transcription of SoxS, which is another transcription promoter that induces the transcription of many genes involved in oxygen detoxification. OxyR and PerR are transcription factors involved in responses to exposure to hydrogen peroxide.

In many anaerobic organisms there exists a different counteraction to exposure to reactive oxygen intermediates where SOD and catalases have been replaced by another system involving distinct enzymes that catalyze the removal of these intermediates in a different manner (*37*). These enzymes are termed superoxide reductase (SOR) and rubrerythrin (Rbr), while there are some oxygen sensitive microorganisms that still contain superoxide dismutases, these are all of the iron type (*38*). SOR was shown to catalyze the reduction of superoxide to hydrogen peroxide (*39*). This work determined that the enzyme was different from superoxide dismutase in that there was no molecular oxygen generated. This enzyme showed 40% and 50% sequence identity to two other redox enzymes previously termed desulfoferrodoxin and neelaredoxin (*40*). In the original assay of SOD, the system involved xanthine and xanthine oxidase that produced superoxide, which would then reduce horse heart cytochrome c if the SOD enzyme was absent. When superxoxide dismutase was added the reduction of cytochrome c would decrease in a manner proportional to the amount of SOD added. A similar reaction was noticed when the enzyme from *P. furiosus* was added in increasing amounts, as the reduction of cytochrome c decreased in a proportional manner. But there was a major difference in the two assays when an

excess of enzyme was added to the reaction mixture. When superoxide dismutase was added in excess, cytochrome c reduction was completely avoided, yet when an excess of the neelaredoxin-like enzyme from *P. furiosus* was added oxidation of cytochrome c was observed, meaning that the neelaredoxin-like enzyme from *P. furiosus* could accept electrons from cytochrome c, yet when only chemically reduced cytochrome c was added the same enzyme would not oxidize it. This phenomenon could only be possible if the enzyme from *P. furiosus* could use cytochrome c as an electron donor in a reaction that involved superoxide. The following reaction and the name, cytochrome c superoxide oxidoreductase, were proposed (Eq. - 6):

$$O_2^- + 2H^+ + 4\text{cyt } c_{red} \longrightarrow H_2O_2 + 4\text{cyt } c_{ox} \quad (6)$$

When an acetylated form of cytochrome c was used in the assay it was shown that the activity decreased 98% and it was thought that this was indicative of an interference with protein-protein interactions. The authors then tested the electron carrier protein, rubredoxin, which is very close to superoxide reductase on the genome of *P. furiosus* as a possible donor for the reduction of superoxide to hydrogen peroxide. Rubredoxin was oxidized when superoxide was added but addition of superoxide reductase increased the oxidation rate and rubredoxin was shown to be the donor for the reaction, which is as follows (Eq. - 7):

$$O_2^- + 2H^+ + 2Rd_{red} \longrightarrow H_2O_2 + 2Rd_{ox} \quad (7)$$

It was also shown that the electrons that ultimately reduce superoxide come from NADPH-rubredoxin oxidoreductase (NROR) via rubredoxin and the scheme in figure 1.4 was developed.

Interesting to note is that SOR shows measureable catalytic activity at temperatures 75°C lower than the optimum growth temperature of this organism. If one considers that this organism grows in deep sea hydrothermal vents and the fact that currents can either sweep it away from the anaerobic environment or cause a temperature fluctuation near the vent, this catalytic feature

of the enzyme becomes quite important. Thus it was understood how superoxide was removed from the cell but one major question remains, "What happens to the hydrogen peroxide?"

The identification of two enzymes with peroxidase activity in an anaerobe was first demonstrated using the anaerobic sulfate reducing bacterium *Desulfovibrio vulgaris* as well as *Clostridium perfringens* in 1999 (*41*). In this work it was shown that a system containing NADH, hydrogen peroxide and a bacterial NADH oxidoreductase could remove hydrogen peroxide. The two enzymes from *D. vulgaris* are termed rubrerythrin and nigerythrin. Nigerythrin was so named because of its deep black color upon purification where the root of its name stems from that of its closely related paralog rubrerythrin. Rubrerythrin was first discovered in *D. vulgaris* and later experiments showed that the enzyme contained a rubredoxin-like iron coordination site and a hemerythrin like di-iron coordination site (*42, 43*). The name of the enzyme was conceived when the two domains were characterized and it was subsequently given a moniker to reflect these two iron coordination motifs. Since the original purification and characterization, enzymatic activities such as pyrophosphatase, ferroxidase, and superoxide dismutase have been reported (*44-46*). It was not until 2004 that the specific role of rubrerythrin was elucidated in a system which used enzymes and cofactors from the same organism (*47*). The rubrerythrin was shown to not have any of the previously mentioned activities and therefore rubredoxin dependent NADH: hydrogen peroxide peroxidase was determined to be the exclusive activity of this enzyme. A more complete understanding of the removal of reactive oxygen intermediates in anaerobes therefore became apparent. The metal constitution of rubrerythrin was debated for quite some time until this work was published. Previous experiments showed that the metal sites could be occupied by either iron or zinc and various activities were retained depending on the metal present (*32, 48-50*). The distinguishing feature of *P. furiosus*

rubrerythrin is that it must retain iron in all three metal sites in order for it to have activity. When the redox cycling enzyme NROR is used, which provides reductant from NADPH oxidation and is also used in the regeneration of reducing equivalents for superoxide reductase, the complete system for reduction of hydrogen peroxide to water using electrons from NADH exists and the above reaction scheme for the complete removal of reactive oxygen species in *P. furiosus* was altered as shown in Figure 1.5.

Recently, work was done in *P. furiosus* with microarray analysis to determine what genes were upregulated upon exposure to hydrogen peroxide (*51*). It is already known that the open reading frames for superoxide reductase and rubrerythrin are transcribed at high levels when the organism is grown under anaerobic conditions (*52*). The growing cultures of *P. furiosus* were exposed to 0.5mM of H_2O_2 and microarray analysis was carried out showing that the ORFs for these two genes were not significantly regulated under the stress condition, indicating that these genes are not part of a response but more of a defense.

Understanding the structure/function relationship of rubrerythrin

Rubrerythrin is a homodimeric enzyme composed of two four-helix bundles each containing a non-cysteine, non-heme di-iron site where all ligands for the iron atoms are composed of glutamate or histidine side chains (*53-55*). The homodimeric enzyme also contains two rubredoxin-like sites wherein each site is composed of four cysteine residues that coordinate the mononuclear iron atom. In the case of *P. furiosus* rubrerythrin, the four-helix bundle is constructed by two peptides that display domain swapping such that two of the four helices come from two different peptide chains (*56*). Recently, the structure of sulerythrin from the strictly aerobic, thermoacidophilic archaeon *Sulfolobus todokaii* has been solved and it displays the domain swapping feature as well, but this enzyme does not contain the rubredoxin-like metal site

nor is it oxygen sensitive (*57*). *S. todokaii* grows optimally at 80°C so the domain swapping feature may be attributed to thermal stability (*58*). The only other crystal structures of rubrerythrin determined to date are from the mesophilic bacterium *D. vulgaris* and do not show the domain swapping feature (*48, 49, 54, 55*). The most recent structures of the enzyme were of a higher resolution reduced form (PDB ID 1LKO), the oxidized form (PDB ID 1LKM), and the oxidized form with azide occupying the active site (PDB ID 1LKP). In a comparison of the reduced and oxidized structures of the *D. vulgaris* enzyme, a movement of one iron atom in the di-iron site increased the inter-iron distance from 3.3 to 4Å as well as ligand switching from glutamate to histidine due to a 1.8Å movement away from histidine toward glutamate during the conversion from the diferrous state to the ([Fe(II), Fe(III)]) mixed-valent state. In the azide-treated structure, great insight was given into the mechanism for hydrogen peroxide reduction to water by the position of the azide molecule in the di-iron active site of the oxidized form. The azide molecule is coordinated by the di-iron site in a cis μ-1,3 fashion, replacing two solvent ligands observed in the reduced form. The coordination of the azide molecule taken with the movement of the iron atom in the di-iron site and ENDOR spectroscopy lead to a mechanism where the mixed-valent state is seen prior to release of the product (*54, 59, 60*). The redox dependent features of the structure of *P. furiosus* rubrerythrin have not been studied as the only crystal structure that exists is a form where zinc has replaced iron. In addition, a distinguishing feature of the enzyme from *P. furiosus* is that when exposed to oxygen, or when 10 molar equivalents of hydrogen peroxide or ferricyanide are added, it immediately precipitates, but the precipitation can be easily reversed by the addition of the reductant sodium dithionite in an anaerobic environment (*47*). Considering the previously determined similarities and differences between the *P. furiosus* and *D. vulgaris* enzymes, further crystallographic studies of the *P.*

furiosus produced enzyme were pursued in order to gain a better understanding of how this enzyme differs structurally under native conditions and the results of this study are discussed in chapters 3 and 4.

Figure 1.1 The phylogenetic tree based on 16s rRNA depicting an emphasis on hyperthermophilic organisms shown with bold lines. Modified from (*61*).

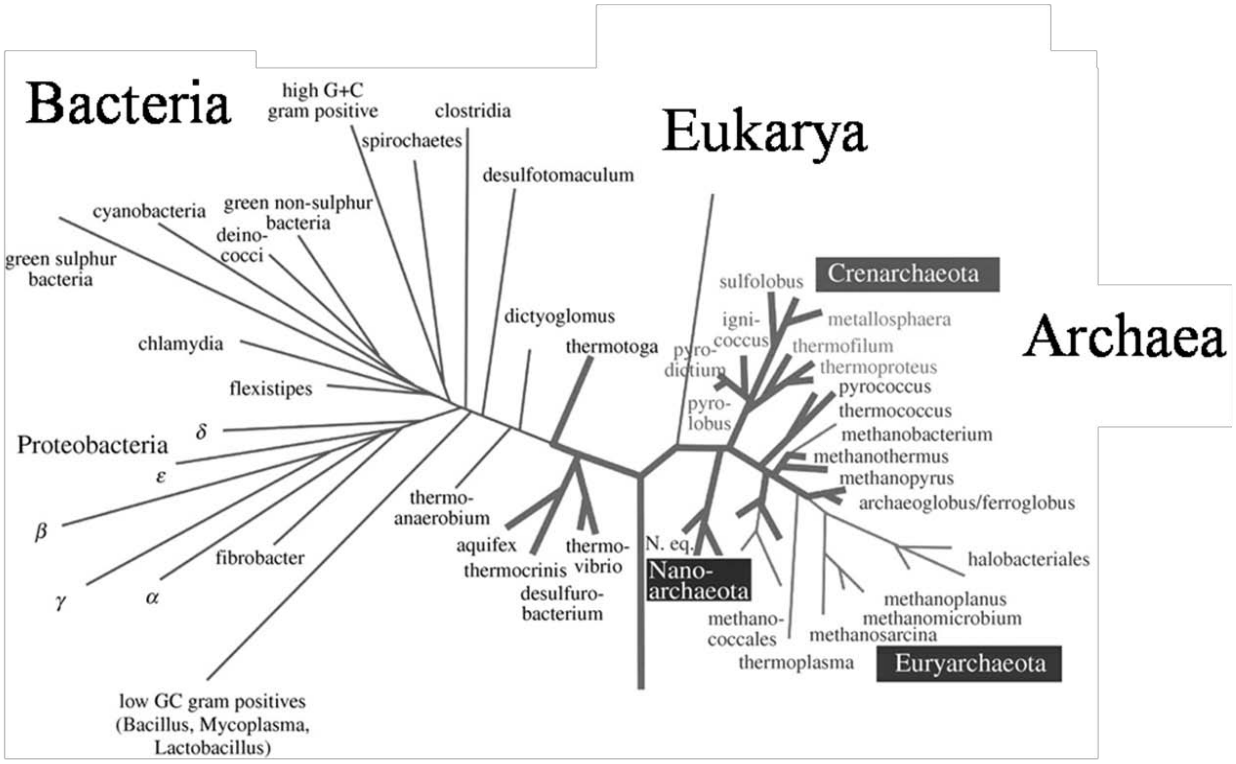
Bacteria
high G+C
gram positive
clostridia
spirochaetes
Eukarya
desulfotomaculum
cyanobacteria
green non-sulphur
bacteria
deino-
cocci
green sulphur
bacteria
sulfolobus
Crenarchaeota
dictyoglomus
igni-
coccus
metallosphaera
Archaea
chlamydia
thermotoga
pyro-
dictium
thermofilum
thermoproteus
flexistipes
pyrococcus
pyro-
lobus
thermococcus
Proteobacteria
δ
methanobacterium
methanothermus
ε
methanopyrus
archaeoglobus/ferroglobus
thermo-
anaerobium
β
aquifex
thermocrinis
thermo-
vibrio
N. eq.
halobacteriales
fibrobacter
Nano-
archaeota
desulfuro-
bacterium
methanoplanus
methanomicrobium
γ
α
methano-
coccales
methanosarcina
thermoplasma
Euryarchaeota
low GC gram positives
(Bacillus, Mycoplasma,
Lactobacillus)

Figure 1.2 Scanning electron micrograph of *P. furiosus* at 30,000x. The flagella have been sheered away by sample preparation. Some of the cells are actively undergoing cell division at different stages. Image courtesy of S. Brehm.

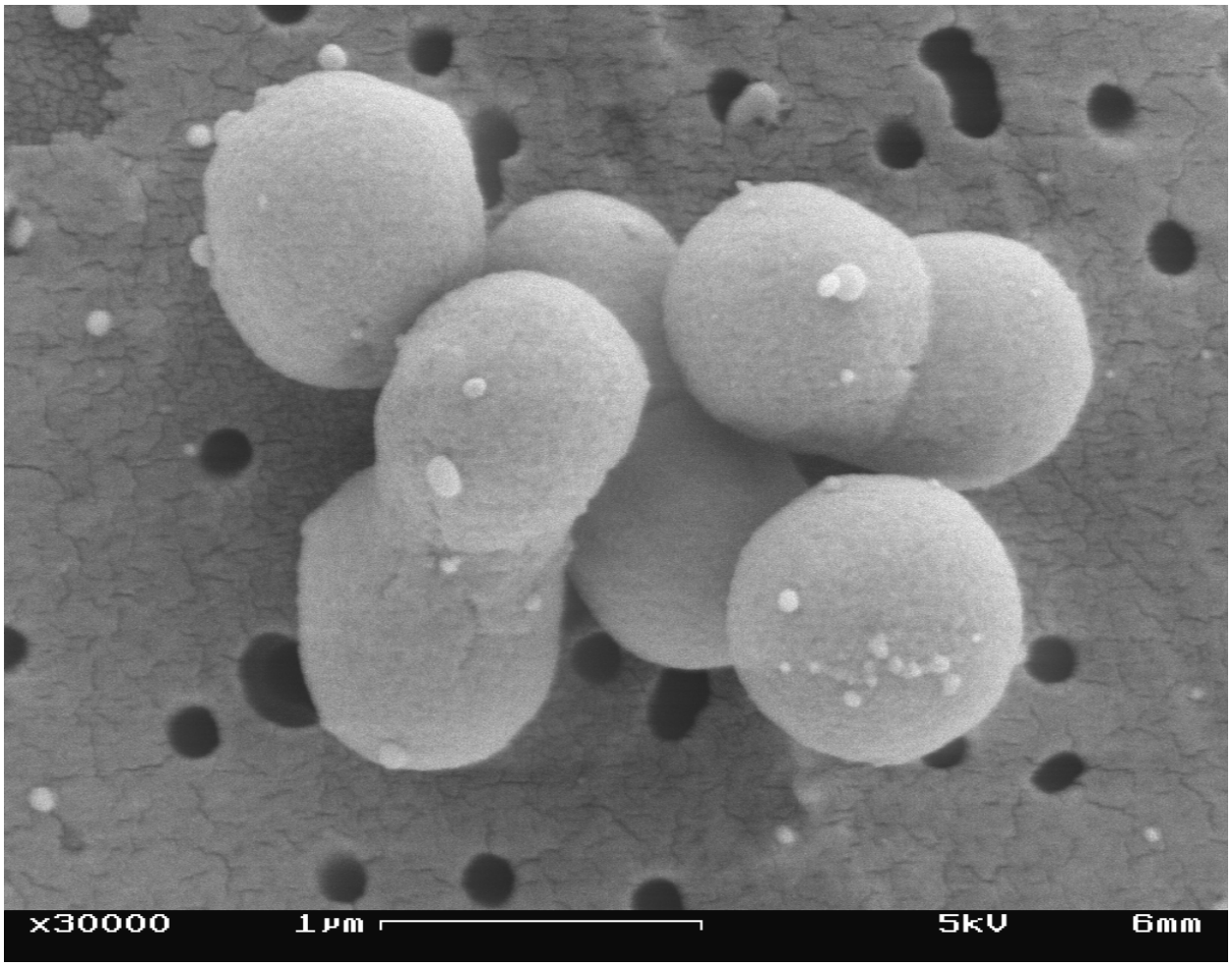
x30000
1μm
5kV
6mm

Figure 1.3 The overall scheme of consumption of peptides depicting the enzymes involved in creation of reducing equivalents and ATP shown in bold. Redrawn from (*62*).

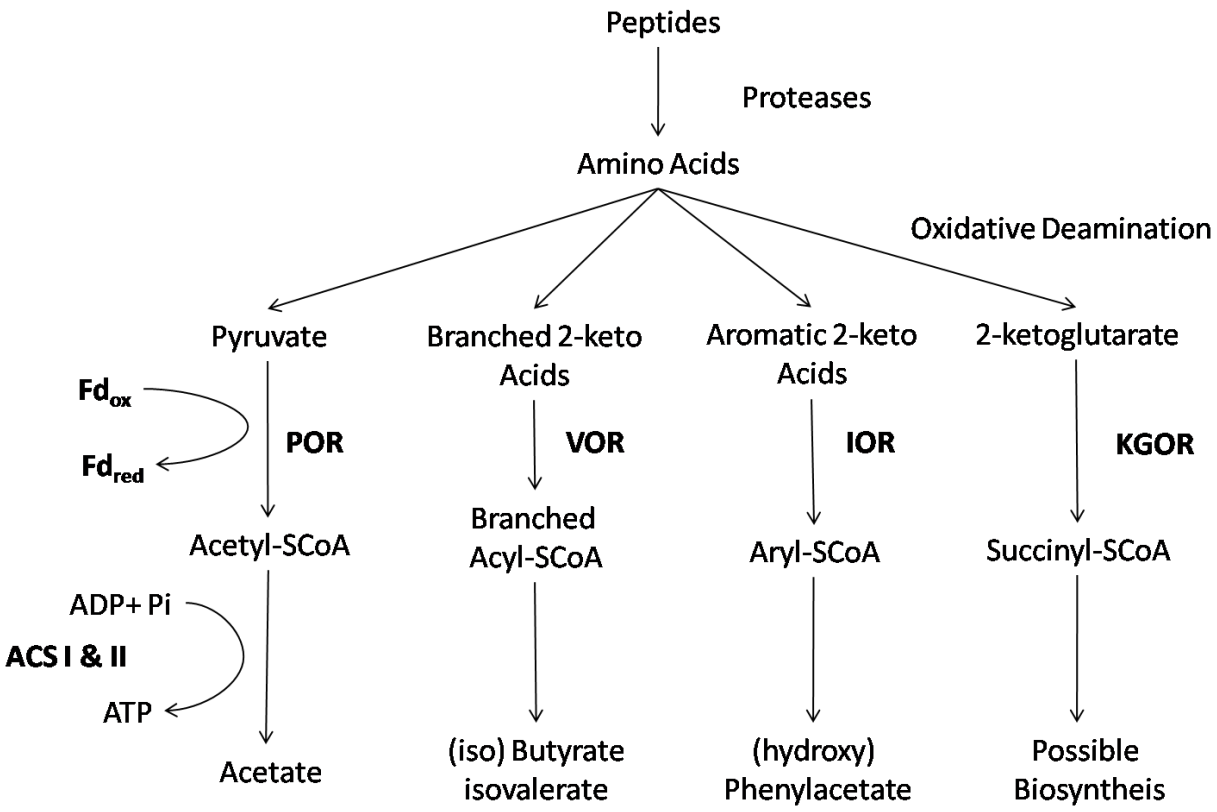
Peptides
Proteases
Amino Acids
Oxidative Deamination
Pyruvate
Branched 2-keto Acids
Aromatic 2-keto Acids
2-ketoglutarate
Fdox
Fdred
POR
VOR
IOR
KGOR
Acetyl-SCoA
Branched Acyl-SCoA
Aryl-SCoA
Succinyl-SCoA
ADP+ Pi
ACS I & II
ATP
Acetate
(iso) Butyrate isovalerate
(hydroxy) Phenylacetate
Possible Biosyntheis

Figure 1.4 Superoxide reductase activities discovered in *P. furiosus*. Redrawn from (*39*)

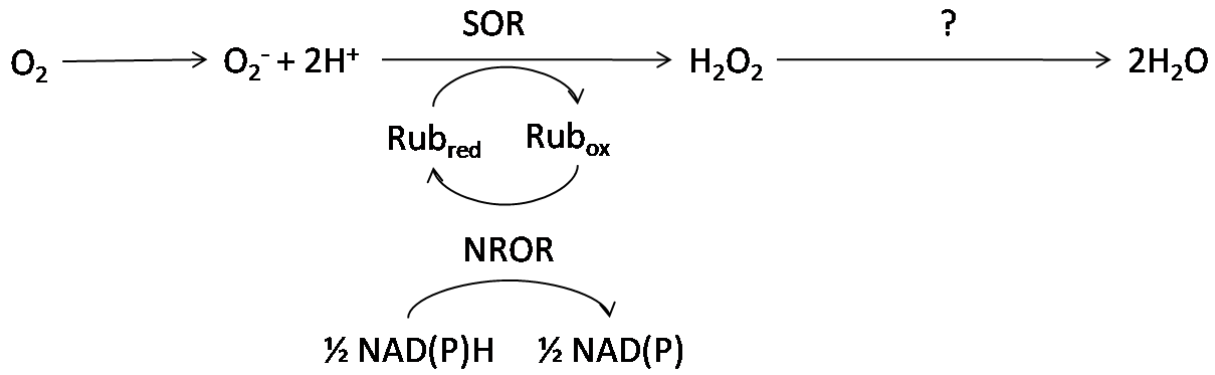
O2
O2- + 2H+
SOR
H2O2
?
2H2O
Rubred
Rubox
NROR
½ NAD(P)H
½ NAD(P)

Figure 1.5 The complete removal of reactive oxygen species from *P. furiosus*. Redrawn from (*47*).

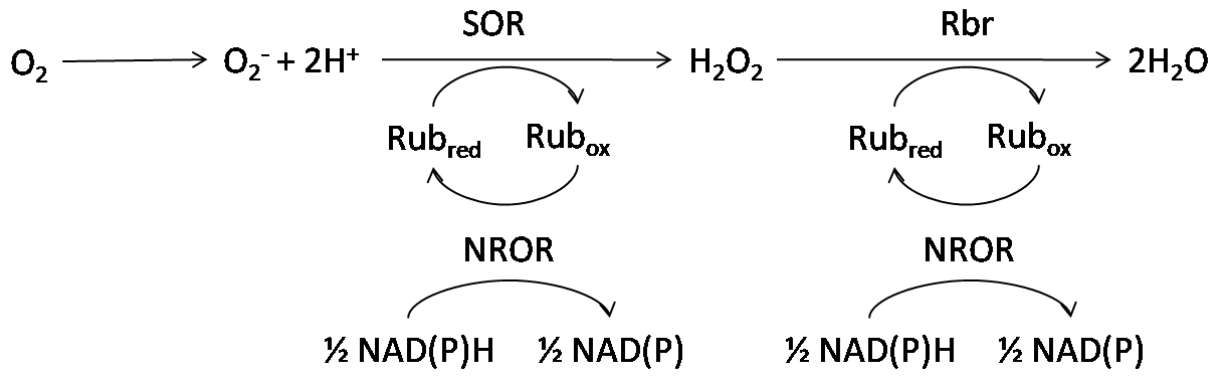
O2
O2- + 2H+
SOR
Rubred
Rubox
NROR
½ NAD(P)H
½ NAD(P)
H2O2
Rbr
Rubred
Rubox
NROR
½ NAD(P)H
½ NAD(P)
2H2O

References

1. Woese, C. R., Kandler, O., and Wheelis, M. L. (1990) Towards a natural system of organisms: proposal for the domains Archaea, Bacteria, and Eucarya, *Proc. Natl. Acad. Sci. USA 87*, 4576-4579.
2. Woese, C. (1998) The universal ancestor, *Proc Natl Acad Sci U S A 95*, 6854-6859.
3. DeLong, E. F. (1998) Everything in moderation: archaea as 'non-extremophiles', *Curr Opin Genet Dev 8*, 649-654.
4. Pikuta, E. V., Hoover, R. B., and Tang, J. (2007) Microbial extremophiles at the limits of life, *Crit Rev Microbiol 33*, 183-209.
5. Barns, S. M., Delwiche, C. F., Palmer, J. D., and Pace, N. R. (1996) Perspectives on archaeal diversity, thermophily and monophyly from environmental rRNA sequences, *Proc Natl Acad Sci U S A 93*, 9188-9193.
6. Elkins, J. G., Podar, M., Graham, D. E., Makarova, K. S., Wolf, Y., Randau, L., Hedlund, B. P., Brochier-Armanet, C., Kunin, V., Anderson, I., Lapidus, A., Goltsman, E., Barry, K., Koonin, E. V., Hugenholtz, P., Kyrpides, N., Wanner, G., Richardson, P., Keller, M., and Stetter, K. O. (2008) A korarchaeal genome reveals insights into the evolution of the Archaea, *Proc Natl Acad Sci U S A 105*, 8102-8107.
7. Huber, R., and Stetter, K. O. (2001) Discovery of hyperthermophilic microorganisms, *Methods Enzymol 330*, 11-24.
8. Takai, K., Nakamura, K., Toki, T., Tsunogai, U., Miyazaki, M., Miyazaki, J., Hirayama, H., Nakagawa, S., Nunoura, T., and Horikoshi, K. (2008) Cell proliferation at 122 degrees C and isotopically heavy CH4 production by a hyperthermophilic methanogen under high-pressure cultivation, *Proc Natl Acad Sci U S A 105*, 10949-10954.
9. Jannasch, H. W., Wirsen, C. O., Molyneaux, S. J., and Langworthy, T. A. (1992) Comparative physiological-studies on hyperthermophilic archaea isolated from deep-sea hot vents with emphasis on *Pyrococcus s*train Gb-D, *Applied and Environmental Microbiology 58*, 3472-3481.
10. A. Koschinsky, C. D. (2006-05-22) Deep-Sea Heat Record: Scientists Observe Highest Temperature Ever Registered at the Sea Floor International University Bremen. wwwback.jacobs-university.de/news/iubnews/09634/.
11. Adams, M. W., Holden, J. F., Menon, A. L., Schut, G. J., Grunden, A. M., Hou, C., Hutchins, A. M., Jenney, F. E., Jr., Kim, C., Ma, K., Pan, G., Roy, R., Sapra, R., Story, S. V., and Verhagen, M. F. (2001) Key role for sulfur in peptide metabolism and in regulation of three hydrogenases in the hyperthermophilic archaeon *Pyrococcus furiosus*, *J Bacteriol 183*, 716-724.
12. Story, S. V., Shah, C., Jenney, F. E., and Adams, M. W. W. (2005) Characterization of a novel zinc-containing, lysine-specific aminopeptidase from the hyperthermophilic archaeon *Pyrococcus furiosus*, *Journal of Bacteriology 187*, 2077-2083.
13. Cheng, T. C., Ramakrishnan, V., and Chan, S. I. (1999) Purification and characterization of a cobalt-activated carboxypeptidase from the hyperthermophilic archaeon *Pyrococcus furiosus*, *Protein Sci 8*, 2474-2486.
14. Tsunasawa, S., Nakura, S., Tanigawa, T., and Kato, I. (1998) Pyrrolidone carboxyl peptidase from the hyperthermophilic archaeon *Pyrococcus furiosus*: cloning and

overexpression in *Escherichia coli* of the gene, and its application to protein sequence analysis, *J Biochem 124*, 778-783.
15. Schut, G. J., Menon, A. L., and Adams, M. W. (2001) 2-keto acid oxidoreductases from *Pyrococcus furiosus* and *Thermococcus litoralis*, *Methods Enzymol 331*, 144-158.
16. Heider, J., Mai, X. H., and Adams, M. W. W. (1996) Characterization of 2-ketoisovalerate ferredoxin oxidoreductase, a new and reversible coenzyme A-dependent enzyme involved in peptide fermentation by hyperthermophilic archaea, *Journal of Bacteriology 178*, 780-787.
17. Mai, X. H., and Adams, M. W. W. (1996) Characterization of a fourth type of 2-keto acid-oxidizing enzyme from a hyperthermophilic archaeon: 2-ketoglutarate ferredoxin oxidoreductase from *Thermococcus litoralis*, *Journal of Bacteriology 178*, 5890-5896.
18. Mai, X. H., and Adams, M. W. W. (1994) Indolepyruvate ferredoxin oxidoreductase from the hyperthermophilic archaeon *Pyrococcus furiosus* - a new enzyme involved in peptide fermentation, *Journal of Biological Chemistry 269*, 16726-16732.
19. Blamey, J. M., and Adams, M. W. W. (1993) Purification and characterization of pyruvate ferredoxin oxidoreductase from the hyperthermophilic archaeon *Pyrococcus furiosus*, *Biochimica Et Biophysica Acta 1161*, 19-27.
20. Ma, K., Hutchins, A., Sung, S. J. S., and Adams, M. W. W. (1997) Pyruvate ferredoxin oxidoreductase from the hyperthermophilic archaeon, *Pyrococcus furiosus*, functions as a CoA-dependent pyruvate decarboxylase, *Proceedings of the National Academy of Sciences of the United States of America 94*, 9608-9613.
21. Mai, X., and Adams, M. W. (1996) Purification and characterization of two reversible and ADP-dependent acetyl coenzyme A synthetases from the hyperthermophilic archaeon *Pyrococcus furiosus*, *J Bacteriol 178*, 5897-5903.
22. van Vugt-Lussenburg, B. M., van der Weel, L., Hagen, W. R., and Hagedoorn, P. L. (2009) Identification of two [4Fe-4S]-cluster-containing hydro-lyases from Pyrococcus furiosus, *Microbiology 155*, 3015-3020.
23. Grant, J. J., and Loake, G. J. (2000) Role of reactive oxygen intermediates and cognate redox signaling in disease resistance, *Plant Physiology 124*, 21-29.
24. Imlay, J. A. (2002) How oxygen damages microbes: Oxygen tolerance and obligate anaerobiosis, *Advances in Microbial Physiology, Vol 46 46*, 111-153.
25. Ligeza, A., Tikhonov, A. N., Hyde, J. S., and Subczynski, W. K. (1998) Oxygen permeability of thylakoid membranes: electron paramagnetic resonance spin labeling study, *Biochimica Et Biophysica Acta-Bioenergetics 1365*, 453-463.
26. Massey, V., Strickla.S, Mayhew, S. G., Howell, L. G., Engel, P. C., Matthews, R. G., Schuman, M., and Sullivan, P. A. (1969) Production of superoxide anion radicals in reaction of reduced flavins and flavoproteins with molecular oxygen, *Biochemical and Biophysical Research Communications 36*, 891-&.
27. Imlay, J. A. (2008) Cellular defenses against superoxide and hydrogen peroxide, *Annual Review of Biochemistry 77*, 755-776.
28. Seaver, L. C., and Imlay, J. A. (2004) Are respiratory enzymes the primary sources of intracellular hydrogen peroxide?, *Journal of Biological Chemistry 279*, 48742-48750.
29. Liochev, S. I., and Fridovich, I. (1994) The Role of O-2-Center-Dot- in the Production of Ho-Center-Dot - in-Vitro and in-Vivo, *Free Radical Biology and Medicine 16*, 29-33.

30. Henle, E. S., Han, Z. X., Tang, N., Rai, P., Luo, Y. Z., and Linn, S. (1999) Sequence-specific DNA cleavage by Fe2+-mediated fenton reactions has possible biological implications, *Journal of Biological Chemistry 274*, 962-971.
31. Yamazaki, I., and Piette, L. H. (1991) Epr spin-trapping study on the oxidizing species formed in the reaction of the ferrous ion with hydrogen-peroxide, *Journal of the American Chemical Society 113*, 7588-7593.
32. Benov, L., Chang, L. Y., Day, B., and Fridovich, I. (1995) Copper, Zinc Superoxide-Dismutase in Escherichia-Coli - Periplasmic Localization, *Archives of Biochemistry and Biophysics 319*, 508-511.
33. Greenberg, J. T., Monach, P., Chou, J. H., Josephy, P. D., and Demple, B. (1990) Positive Control of a Global Antioxidant Defense Regulon Activated by Superoxide-Generating Agents in *Escherichia-Coli*, *Proceedings of the National Academy of Sciences of the United States of America 87*, 6181-6185.
34. Fabrega, A., Martin, R. G., Rosner, J. L., Tavio, M. M., and Vila, J. (2010) Constitutive SoxS expression in a fluoroquinolone-resistant strain with a truncated SoxR protein and identification of a new member of the marA-soxS-rob regulon, mdtG, *Antimicrobial Agents and Chemotherapy 54*, 1218-1225.
35. Christman, M. F., Morgan, R. W., Jacobson, F. S., and Ames, B. N. (1985) Positive control of a regulon for defenses against oxidative stress and some heat-shock proteins in *Salmonella typhimurium*, *Cell 41*, 753-762.
36. King, K. Y., Horenstein, J. A., and Caparon, M. G. (2000) Aerotolerance and peroxide resistance in peroxidase and PerR mutants of *Streptococcus pyogenes*, *Journal of Bacteriology 182*, 5290-5299.
37. Brioukhanov, A. L., and Netrusov, A. I. (2004) Catalase and superoxide dismutase: distribution, properties, and physiological role in cells of strict anaerobes, *Biochemistry (Mosc) 69*, 949-962.
38. Kirschvink, J. L., Gaidos, E. J., Bertani, L. E., Beukes, N. J., Gutzmer, J., Maepa, L. N., and Steinberger, R. E. (2000) Paleoproterozoic snowball earth: extreme climatic and geochemical global change and its biological consequences, *Proc Natl Acad Sci U S A 97*, 1400-1405.
39. Jenney, F. E., Jr., Verhagen, M. F., Cui, X., and Adams, M. W. (1999) Anaerobic microbes: oxygen detoxification without superoxide dismutase, *Science 286*, 306-309.
40. Niviere, V., and Fontecave, M. (2004) Discovery of superoxide reductase: an historical perspective, *J Biol Inorg Chem 9*, 119-123.
41. Coulter, E. D., Shenvi, N. V., and Kurtz, D. M., Jr. (1999) NADH peroxidase activity of rubrerythrin, *Biochem Biophys Res Commun 255*, 317-323.
42. LeGall, J., Prickril, B. C., Moura, I., Xavier, A. V., Moura, J. J., and Huynh, B. H. (1988) Isolation and characterization of rubrerythrin, a non-heme iron protein from *Desulfovibrio vulgaris* that contains rubredoxin centers and a hemerythrin-like binuclear iron cluster, *Biochemistry 27*, 1636-1642.
43. Pierik, A. J., Wolbert, R. B., Portier, G. L., Verhagen, M. F., and Hagen, W. R. (1993) Nigerythrin and rubrerythrin from *Desulfovibrio vulgaris* each contain two mononuclear iron centers and two dinuclear iron clusters, *Eur J Biochem 212*, 237-245.

44. Gupta, N., Bonomi, F., Kurtz, D. M., Jr., Ravi, N., Wang, D. L., and Huynh, B. H. (1995) Recombinant *Desulfovibrio vulgaris* rubrerythrin. Isolation and characterization of the diiron domain, *Biochemistry 34*, 3310-3318.
45. Lehmann, Y., Meile, L., and Teuber, M. (1996) Rubrerythrin from *Clostridium perfringens*: cloning of the gene, purification of the protein, and characterization of its superoxide dismutase function, *J Bacteriol 178*, 7152-7158.
46. Liu, M. Y., and Le Gall, J. (1990) Purification and characterization of two proteins with inorganic pyrophosphatase activity from *Desulfovibrio vulgaris*: rubrerythrin and a new, highly active, enzyme, *Biochem Biophys Res Commun 171*, 313-318.
47. Weinberg, M. V., Jenney, F. E., Jr., Cui, X., and Adams, M. W. (2004) Rubrerythrin from the hyperthermophilic archaeon *Pyrococcus furiosus* is a rubredoxin-dependent, iron-containing peroxidase, *J Bacteriol 186*, 7888-7895.
48. Jin, S., Kurtz, D. M., Jr., Liu, Z. J., Rose, J., and Wang, B. C. (2004) Displacement of iron by zinc at the diiron site of *Desulfovibrio vulgaris* rubrerythrin: X-ray crystal structure and anomalous scattering analysis, *J Inorg Biochem 98*, 786-796.
49. Jin, S., Kurtz, D. M., Jr., Liu, Z. J., Rose, J., and Wang, B. C. (2004) X-ray crystal structure of *Desulfovibrio vulgaris* rubrerythrin with zinc substituted into the [Fe(SCys)4] site and alternative diiron site structures, *Biochemistry 43*, 3204-3213.
50. Li, M., Liu, M. Y., LeGall, J., Gui, L. L., Liao, J., Jiang, T., Zhang, J. P., Liang, D. C., and Chang, W. R. (2003) Crystal structure studies on rubrerythrin: enzymatic activity in relation to the zinc movement, *J Biol Inorg Chem 8*, 149-155.
51. Strand K. R., S. C., Li T., Jenney, Jr. F. E., Schut G. J., Adams M. W. W. . (To be published 2010) Oxidative stress protection and the repair response to hydrogen peroxide in the hyperthermophilic archaeon *Pyrococcus furiosus* and in related species *Arch. Microbiol.*
52. Schut, G. J., Brehm, S. D., Datta, S., and Adams, M. W. (2003) Whole-genome DNA microarray analysis of a hyperthermophile and an archaeon: *Pyrococcus furiosus* grown on carbohydrates or peptides, *J Bacteriol 185*, 3935-3947.
53. deMare, F., Kurtz, D. M., Jr., and Nordlund, P. (1996) The structure of *Desulfovibrio vulgaris* rubrerythrin reveals a unique combination of rubredoxin-like FeS4 and ferritin-like diiron domains, *Nat Struct Biol 3*, 539-546.
54. Jin, S., Kurtz, D. M., Jr., Liu, Z. J., Rose, J., and Wang, B. C. (2002) X-ray crystal structures of reduced rubrerythrin and its azide adduct: a structure-based mechanism for a non-heme diiron peroxidase, *J Am Chem Soc 124*, 9845-9855.
55. Sieker, L. C., Holmes, M., Le Trong, I., Turley, S., Liu, M. Y., LeGall, J., and Stenkamp, R. E. (2000) The 1.9 A crystal structure of the "as isolated" rubrerythrin from *Desulfovibrio vulgaris*: some surprising results, *J Biol Inorg Chem 5*, 505-513.
56. Tempel, W., Liu, Z. J., Schubot, F. D., Shah, A., Weinberg, M. V., Jenney, F. E., Jr., Arendall, W. B., 3rd, Adams, M. W., Richardson, J. S., Richardson, D. C., Rose, J. P., and Wang, B. C. (2004) Structural genomics of *Pyrococcus furiosus*: X-ray crystallography reveals 3D domain swapping in rubrerythrin, *Proteins 57*, 878-882.
57. Fushinobu, S., Shoun, H., and Wakagi, T. (2003) Crystal structure of sulerythrin, a rubrerythrin-like protein from a strictly aerobic archaeon, Sulfolobus tokodaii strain 7, shows unexpected domain swapping, *Biochemistry 42*, 11707-11715.

58. Wakagi, T. (2003) Sulerythrin, the smallest member of the rubrerythrin family, from a strictly aerobic and thermoacidophilic archaeon, *Sulfolobus tokodaii* strain 7, *FEMS Microbiol Lett 222*, 33-37.
59. Iyer, R. B., Silaghi-Dumitrescu, R., Kurtz, D. M., Jr., and Lanzilotta, W. N. (2005) High-resolution crystal structures of *Desulfovibrio vulgaris* (Hildenborough) nigerythrin: facile, redox-dependent iron movement, domain interface variability, and peroxidase activity in the rubrerythrins, *J Biol Inorg Chem 10*, 407-416.
60. Smoukov, S. K., Davydov, R. M., Doan, P. E., Sturgeon, B., Kung, I. Y., Hoffman, B. M., and Kurtz, D. M., Jr. (2003) EPR and ENDOR evidence for a 1-His, hydroxo-bridged mixed-valent diiron site in Desulfovibrio vulgaris rubrerythrin, *Biochemistry 42*, 6201-6208.
61. Stetter, K. O. (2006) History of discovery of the first hyperthermophiles, *Extremophiles 10*, 357-362.
62. Adams, M. W., and Kletzin, A. (1996) Oxidoreductase-type enzymes and redox proteins involved in fermentative metabolisms of hyperthermophilic Archaea, *Adv Protein Chem 48*, 101-180.

CHAPTER 2

PROLINE DEHYDROGENASE 1 FROM *PYROCOCCUS FURIOSUS* CONTAINS A REDOX ACTIVE 2FE-2S CLUSTER[1]

[1]Bret D. Dillard, Gerrit J. Schut, Aleksandar Cvetkovic, Sowmya Subramanian, Michael Johnson, and M. W. W. Adams. 2010. (To be submitted to *Biochemistry*)

ABSTRACT

Proline dehydrogenase 1 (PDH1) catalyzes the oxidation of proline to pyrroline-5-carboxylate. PDH1 from the hyperthermophilic archaeon *Pyrococcus furiosus* DSM 3638 has been purified from native biomass under strict anaerobic conditions. The enzyme is a heterodimer with subunits of 54 and 42 kDa. It is brown in color and contains 2.3 ± 0.2 iron atoms per heterodimer (96 kDa). The two genes encoding PDH1 (PF1245 and PF1246) were cloned and expressed in *Escherichia coli.* The recombinant protein was purified under strictly anaerobic conditions and contained 1.6 ± 0.2 iron atoms per heterodimer. Electron paramagnetic resonance (EPR) analysis indicates that the recombinant enzyme contains a [2Fe-2S] cluster that is reduced by treatment with proline or sodium dithionite. A screen of artificial electron acceptors showed that resorufin (-51mV) and 2,6-dichloroinophenol (DCIP) (+217mV) were reduced by the protein using proline as an electron donor. Exposure of the enzyme to air for 15 minutes resulted in visible bleaching and loss of the iron-sulfur cluster. The air-treated enzyme showed no loss of activity with DCIP as the electron acceptor but was inactive with resorufin. The enzyme has a K_m for proline of 87 μM at 80°C when resorufin was used as an acceptor, which is two orders of magnitude lower than that measured for proline when DCIP was used. The enzyme does not catalyze the transfer of electrons from proline to potential physiological electron acceptors such as NAD^+, $NADP^+$, rubredoxin or ferredoxin from *P. furiosus*. The results show that the iron-sulfur cluster is an integral part of the physiological electron transfer for proline dehydrogenase 1 in *P. furiosus.*

INTRODUCTION

The enzyme responsible for proline oxidation in mesophilic bacteria, proline utilization A (PutA), has been well characterized. It is a membrane associated bi-functional enzyme that catalyzes the two electron oxidation of proline to pyrroline-5-carboxylate, carried out by the proline dehydrogenase domain, and this is subsequently hydrolyzed to γ-glutamic acid semialdehyde and oxidized by the pyrroline-5-carboxylate dehydrogenase domain in an NAD^+ dependent reaction to generate glutamate and NADH (*1, 2*). In *Escherichia coli* and *Salmonella typhimurium*, the enzyme has been shown to be a transcriptional regulator in response to the levels of proline available (*3, 4*). Thus, it is either functioning as membrane-associated enzyme or a DNA-binding protein acting as a repressor depending on the level of proline present (*3*). The x-ray crystal structure of the proline dehydrogenase domain shows that it forms a $\beta_8\,\alpha_8$ barrel containing a non-covalent flavin adenine dinucleotide cofactor (*5*). It is the redox state of the flavin moeity that determines whether the enzyme is membrane associated or acting as a DNA repressor (*6, 7*).

In hyperthermophilic archaea, proline dehydrogenase activity was originally found in *Thermococcus profundus* and the enzyme was thought to be composed of two distinct gene products (*8*). Through genome analyses it was later shown that a second enzyme of this type was present in this organism and it was composed of four distinct gene products. The alpha and gamma subunits contain a [2Fe-2S] and [8Fe-8S] cluster, respectively based on spectrophotometric analysis of the individual subunits (*9*). In the same work, the alpha subunit was shown to lose the characteristic peak at 340nm due to the [2Fe-2S] cluster gradually upon exposure to air showing that it may be oxygen sensitive. The alpha subunit also exhibited DCIP

dye-linked NADH dehydrogenase activity, but whether the activity remained after exposure to oxygen was not tested.

Genomic and biochemical analyses lead to the discovery of two types of proline dehydrogenase in the related hyperthermophilic archaeon *Pyrococcus horikoshii.* One, termed PDH1, is composed of two distinct gene products with proline dehydrogenase activity and these have high similarity to the alpha and beta subunits of the four subunit enzyme which is termed PDH2 (*10*). PDH1 did not contain an iron-sulfur cluster when purified from *P. horikoshii*, but it was shown to contain flavin adenine dinucleotide, flavin adenine mononucleotide, and adenosine triphosphate (*10*). The genome sequence of the hyperthermophilic archaeon *P. furiosus* shows that it also contains two distinct PDHs that should carry out the oxidation of proline to pyrroline-5-carboxylate, a two subunit form PDH1 (PF1245-PF1246) and a four subunit form PDH2 (PF1795-PF1798) *(11).*

The x-ray crystal structures of PDH1 from *P. horikoshii* and from *P. furiosus* have been determined using enzymes purified under aerobic conditions with activity determined using DCIP as an electron acceptor. The positions of two flavin moieties and their proximity to a cluster of cysteine residues was observed as well as the existence of an ATP molecule which was thought to be regulatory (*11, 12*). That the cluster of cysteine residues might coordinate an iron-sulfur cluster was examined by obtaining the recombinant *P. furiosus* protein from *E. coli* under anaerobic conditions and carrying out the purification anaerobically. However, the purified protein did not contain an iron-sulfur cluster. The purpose of this work was to examine the properties of PDH1 purified from native *P. furiosus* biomass. We show that the enzyme obtained in this fashion contains a [2Fe-2S] cluster and the affinity of the enzyme for proline is two orders of magnitude higher compared to the enzyme lacking the cluster.

MATERIALS AND METHODS

Purification of native (n)PDH1 from *P. furiosus.* Frozen *P. furiosus* cell paste (15 g) grown on peptides in the presence of S^0 was lysed anaerobically by osmotic shock in 200 mL of 50 mM Tris-HCl (pH 8.0) under argon followed by sonication (Branson sonifier, 10 min, power setting 4)(*13*). The cell extract was centrifuged at 100,000 x *g* for 1 h to obtain the cytoplasmic fraction. nPDH1 was purified by anaerobic multistep chromatography using an Akta Basic (GE Healthcare, Piscataway, NJ). Unless otherwise stated, 50 mM Tris-HCl (pH 8.0) buffer was used, and all column chromatography materials were obtained from GE Healthcare. The cytoplasmic fraction (72 mL, 547 mg) was loaded onto a QHP-Sepharose column (30 mL) at a flow rate of 5 mL/min. The column was washed with 10 column volumes (CV) of buffer and the absorbed proteins were eluted with a NaCl gradient (0 to 0.5 M) over 20 CV. nPDH1 eluted as 265 to 310 mM NaCl was applied to the column. The active fractions from the gradient elution step were pooled (60 mL, 22.25 mg), and were loaded onto a Phenyl Sepharose column (5 mL) at a flow rate of 5 mL/min, while being mixed in a 1:1 ratio with 0.8M $(NH_4)_2SO_4$ in 50 mM Tris (pH 8.0) and washed with 2 CV and eluted with decreasing concentrations of $(NH_4)_2SO_4$ (0.8 to 0 M over 20 CV). nPDH1 activity was eluted as 516 to 350 mM $(NH_4)_2SO_4$ was applied. Active fractions were pooled (20 mL, 8.8 mg), diluted threefold with buffer, loaded onto a hydroxyapatite (Bio-Rad) column (7 mL) at a flow rate of 4 mL/min, and washed with 10 CV of buffer containing 5 mM phosphate (pH 7.4). PDH1 eluted when 170 to 209 mM phosphate was applied as part of a linear gradient of phosphate (5 to 500 mM in 20 CV). The nPDH1 samples (10 mL, 1.12 mg) from the hydroxyapatite column were stored at 4°C.

Purification of recombinant (r)PDH1 from *E. coli*. A pET24d plasmid containing PF1245-PF1246 genes cloned in tandem with a His-6 tag (MAHHHHHHGS) at the N terminus of

PF1245 was provided by the Southeastern Collaboratory for Structural Genomics at the University of Georgia. This was transformed into *E. coli* strain BL21 (λDE3)Star/pRIL, (Stratagene). These cells were grown aerobically on 2XYT medium containing 50 µg/mL of kanamycin and 34 µg/mL of chloramphenicol in 2.8-liter Fernbach flasks (1 liter medium) at 37°C for 6 h with shaking at 200 rpm before induction with 1 mM isopropyl-D-thiogalactopyranoside (IPTG). Upon induction 400µM $FeCl_2$ was added and the 1L cultures were combined and transferred to 2L bottles and then stoppered to switch to anaerobic growth. After 16 h at 18°C, cells were harvested (10,000 x *g*, 2 min), resuspended in 100 mL 50 mM Tris-HCl (pH 8.0), degassed under argon, and frozen at -20°C. All purification procedures were carried out under anaerobic conditions, and all chemicals were obtained from Sigma (St. Louis, MO). Frozen cells (18 g) were thawed in the presence of lysozyme (0.2 mg/mL), DNase I (0.5 mg/mL), and phenylmethylsulfonyl fluoride (1 mM) and incubated with shaking at 37°C for 1 h. The cell extract was sonicated (Branson sonifier, 10 min, power setting 4), incubated at 80°C for 30 min, and then centrifuged (40,000 x *g* for 45 min) to remove denatured proteins. The heat-treated cytoplasmic extract containing rPDH1 activity was loaded onto a 12-mL Ni-nitrilotriacetic acid drip column (HIS-Select nickel affinity gel; Sigma) equilibrated with 50 mM Tris-HCl (pH 8.0) containing 0.3 M NaCl. rPDH1, was eluted with 300 mM imidazole in the same buffer. The His-tagged protein was then applied and eluted on a 7mL hydroxyapatite column in the same manner as the native enzyme. The protein that eluted from the hydroxyapatite column was judged pure by SDS-PAGE analysis. The protein in the elution peak was concentrated to 44.3 mg/mL with a specific activity of 0.91 units/mg for ICP-MS and EPR analyses.

Iron Determination. The iron content of nPDH1 and rPDH1 were determined by ICP-MS analysis. Nitric acid, 0.995 mL of 2% (A509-212, Fisher, Canada) was added to each 5µl sample to be analyzed. Samples incubated at 23°C for 1.5h and were clarified by centrifugation at 3500 rpm for 5 minutes prior to analysis by ICP-MS (ICP-MS 7500ce, Agilent Technologies, Tokyo, Japan). The sample was analyzed in triplicate for the content of iron and the internal standard from the sample tube was 1 ppm (prepared diluting 10 ppm of IV-ICPMS-71D solution from Inorganic Ventures ISTD in 2% nitric acid) was added online to the final concentration of 50 ppb. For quantification of results from He mode Li, Sc, and Y were monitored as internal standards, while in no gas mode for this purpose Y, In, and Bi were utilized. External standards were prepared in solution containing 2% nitric acid (mix of CCS-5, CMS-2 and IV-ICPMS-71A from Inorganic Ventures). Data were acquired in FullQuant Mode (3 acquisitions) and analyzed as elements were quantified against an external calibration plot generated from the standards using the internal standard as a reference. The concentrations were corrected for dilution, buffer impact and converted to µM and then compared to the µM amount of protein in the sample.

EPR Analysis of Recombinant PDH1. X-band EPR spectra were recorded on a Bruker Instruments ESP 300D spectrometer equipped with an Oxford Instruments ESR 900 flow cryostat (4.2–300 K). Spectra were quantified under non-saturating conditions by double integration against a 1 mM CuEDTA standard.

Enzyme Assays. For assays using resorufin as the electron carrier, the reaction mixture (2mL) in 2.5mL stoppered glass cuvettes contained 100 mM EPPS, pH 8.4, 5µM FAD and FMN, 100 mM proline, and 120 µM resorufin. The mixture was incubated at 80°C for 3 minutes prior to addition of substrate. Upon addition of the substrate the decrease in absorption at 570nm was monitored. One unit of activity was defined as the amount of enzyme catalyzing the reduction of

1 µmole of resorufin/min. An extinction coefficient at 570nm of 65 $mM^{-1}cm^{-1}$ was used for resorufin (Sigma-Aldrich). Enzyme assays using DCIP as the electron carrier were carried out as previously described, except that the reaction volume was 2mL and all assays were carried out under anaerobic conditions in stoppered cuvettes (*9*). For kinetic analyses using DCIP, FAD and FMN (each 5 µM) were added to the reaction mixture.

Other methods. SDS-polyacrylamide gel electrophoresis analysis of purified nPDH1 and rPDH1 was performed using 4 to 20% Criterion Gels (Biorad) with a Tris buffer system. Samples were heated at 100°C for 10 min prior to loading. Matrix-assisted laser desorption ionization (MALDI) was performed on a Bruker Autoflex (time of flight) mass spectrometer. SDS-polyacrylamide gel electrophoresis gel bands of purified native and recombinant were excised, destained, and dehydrated with 50% acetonitrile in 50 mM NH_4HCO_3 and then digested with 15 µl of 10 µg/mL trypsin for 16 h. Peptides were then extracted from the gel slice by three 15-min washes (once with 50 mM NH_4HCO_3 and twice with 75% acetonitrile, 0.5% trifluoroacetic acid). Peptides were purified using NuTip C18 tips (Glygen Corp., Columbia, MD) and spotted (1 µl, containing α-cyano-4-hydroxycinnamic acid) directly on a matrix-assisted laser desorption ionization plate. Data analysis was performed in Protein Prospector v3.2.1 using MS-Fit (http://prospector.ucsf.edu/). Protein concentrations were determined by total amino acid analysis at the Molecular Structure Facility, UC Davis. K_m and V_{max} values were calculated using the program Prism. Assays to test the effect of different nucleotides on activity were performed using ATP, ADP, GTP, GDP, CTP, and UTP in varying amounts from 0.01mM to 1mM final concentration added to the assay mixes described previously for DCIP and resorufin.

RESULTS and DISCUSSION

Growth Conditions of *P. furiosus* for the Purification of PDH1. Microarray studies of *P. furiosus* have given insight into transcription levels of the genes encoding PDH1 (PF1245-PF1246) and PDH2 (PDH1795-PF1798) under different growth conditions (*14, 15*). Expression of PDH1 is upregulated but PDH2 is not when the organism is grown on peptides and sulfur as compared to growth on maltose or maltose and sulfur (*14, 15*). Proline dehydrogenase activity was measured in the cytoplasmic fraction from maltose, maltose/sulfur, and peptide/sulfur grown cells. The activity of pyruvate ferredoxin oxidoreductase, which is expressed at similar levels in all growth conditions, was used as a control (*14, 15*). Peptide/sulfur grown cells had the highest specific activity for proline dehydrogenase. The activities are reported in Table 1. This information, taken with the microarray data, led to the selection of that growth condition from which to purify PDH1 from *P. furiosus* cells (nPDH1).

Purification of nPDH1 and rPDH1. The two forms of PDH1 were purified under strict anaerobic conditions, which was necessary to preserve the brown color of the enzyme. If nPDH1 or rPDH1 was exposed to oxygen it turned from brown to yellow within minutes, indicative of the loss of the iron-sulfur cluster but the retention of the flavin groups, as suggested previously (*11, 12*). nPDH1 was purified to a specific activity of 0.54 μmoles DCIP reduced/min/mg with a yield of 4.8% which was the result of a 23.3-fold purification. rPDH1 was purified to a specific activity of 0.91 μmoles DCIP reduced/min/mg with a yield of 106%, which was the result of a 24-fold purification. Both nPDH1 and rPDH1 were judged pure by SDS-PAGE analyses (Figure 1) Mass spectrometry was performed on the two subunits of both the native and recombinant proteins and this unambiguously identified the proteins purified as the products of PF1245 and PF1246.

Physical Properties of PDH1. nPDH1 and rPDH1 contained 2.3 ± 0.2 and 1.6 ± 0.2 iron atoms per αβ dimer (96 kDa), respectively, by ICP-MS analysis when purified under strict anaerobic conditions. The X-band EPR spectrum of the as-purified rPDH1 sample comprises a slow-relaxing weak isotropic signal at g = 2.007 accounting for < 0.01 spins/molecule, which is attributed to trace amounts of a flavin semiquinone radical species. In contrast rPDH1 samples treated with proline or sodium dithionite exhibit identical near-axial S =1/2 resonance with g = 2.02, 1.91 and 1.87 at 10 K, that are observable without significant broadening at 70 K (Figure 2). EPR spectra recorded over a wider scan range indicate the absence of any high-spin half-integer species, see Figure 3. Taken together, the g –value anisotropy and the relaxation properties are characteristic of a S = 1/2 $[2Fe\text{-}2S]^{+}$ center rather than a S = 1/2 $[4Fe\text{-}4S]^{+}$ center (*16*). The S = 1/2 resonances in both the dithionite-reduced and proline reduced samples account for 0.15 ± 0.02 spins/molecule indicating that the $[2Fe\text{-}2S]^{2+,+}$ cluster is only partially reduced by dithionite and excess substrate or is present in sub-stoichiometric amounts in the as purified samples of rPDH1. Observation of the signal at temperatures as high as 70 K indicates that the cluster is of the [2Fe-2S] type as signals from a $[4Fe\text{-}4S]^{+}$ would not be observed at those temperatures. Such a conclusion is supported by the measured iron contents of nPDH1 and rPDH1.

Electron carrier specificity of n/rPDH1. The K_m for the electron carrier resorufin with saturating amounts of proline was determined to be ~30 µM and the concentration used in the assays for the determination of the kinetic parameters for proline was 120 µM. Varying amounts of proline were added to anaerobic cuvets and kinetic parameters were determined at different temperatures. The activity of n/rPDH1 using resorufin as an electron carrier was reduced to zero when the enzyme was exposed to air for 15 minutes, even though the enzyme retained 100% of

its activity using DCIP as the carrier. The specific activity and K_m for proline of the enzyme using DCIP (1 mM) at 50°C with the cluster were determined to be 2.1 U/mg and 3800 µM. The specific activity and K_m for proline of the enzyme using DCIP at 50°C without the cluster were determined to be 1.8 U/mg and 4200 µM. These activities are similar to those previously determined for the enzyme lacking the iron-sulfur cluster using DCIP as the electron acceptor (*11*). The specific activity and K_m for proline of the enzyme using resorufin at 50°C with the cluster were determined to be 0.028 U/mg and 27.9 µM while the same measurements at 80°C of the enzyme containing the cluster were 0.094 U/mg and 87.3 µM. The results show that the enzyme has a greater affinity for proline when transferring electrons through the [2Fe-2S] cluster. The K_m values for proline of PDH1 with and without the cluster for both dyes at varying temperatures are shown in Table 4. The possibility that nucleotides could have an effect on activity based on the discovery of ATP bound near the cysteine cluster as seen in the x-ray crystal structure was tested and no affect was observed.

We speculate that the four cysteine residues forming the previously described cluster of residues seen in the x-ray crystal structure instead coordinate a [2Fe-2S] cluster. The cluster is reduced by both proline and dithionite as shown by EPR analysis and electrons are accepted by resorufin only when the iron-sulfur cluster is present. We tested NAD^+, $NADP^+$, *P. furiosus* ferredoxin, and *P. furiosus* rubredoxin as possible electron acceptors but no activity was detected. It is possible that there is another protein involved in electron transfer from proline to the physiologically relevant acceptor. It now appears that the cluster acts as the third cofactor involved in electron transfer. Figure 4 shows the possible route of electron transfer within PDH1. Electrons from proline that reduce FAD are then transferred to FMN, and DCIP could accept electrons from this cofactor. In this work it was shown that a [2Fe-2S] cluster exists and

the electron carrier resorufin specifically is reduced when the iron-sulfur cluster is present. While the physiological electron acceptor for PDH1 was not determined, it is possible that another protein is involved in electron transfer as depicted in Figure 4.

Acknowlegements

We would like to thank Dr. Zachary Wood for the use of computational equipment.

REFERENCES

1. Scarpulla, R. C., and Soffer, R. L. (1978) Membrane-bound proline dehydrogenase from *Escherichia coli*. Solubilization, purification, and characterization, *J Biol Chem 253*, 5997-6001.
2. Menzel, R., and Roth, J. (1981) Purification of the putA gene product. A bifunctional membrane-bound protein from *Salmonella typhimurium* responsible for the two-step oxidation of proline to glutamate, *J Biol Chem 256*, 9755-9761.
3. Menzel, R., and Roth, J. (1981) Regulation of the genes for proline utilization in *Salmonella typhimurium*: autogenous repression by the putA gene product, *J Mol Biol 148*, 21-44.
4. Gu, D., Zhou, Y., Kallhoff, V., Baban, B., Tanner, J. J., and Becker, D. F. (2004) Identification and characterization of the DNA-binding domain of the multifunctional PutA flavoenzyme, *J Biol Chem 279*, 31171-31176.
5. Lee, Y. H., Nadaraia, S., Gu, D., Becker, D. F., and Tanner, J. J. (2003) Structure of the proline dehydrogenase domain of the multifunctional PutA flavoprotein, *Nat Struct Biol 10*, 109-114.
6. Wood, J. M. (1987) Membrane association of proline dehydrogenase in *Escherichia coli* is redox dependent, *Proc Natl Acad Sci U S A 84*, 373-377.
7. Muro-Pastor, A. M., Ostrovsky, P., and Maloy, S. (1997) Regulation of gene expression by repressor localization: biochemical evidence that membrane and DNA binding by the PutA protein are mutually exclusive, *J Bacteriol 179*, 2788-2791.
8. Sakuraba, H., Takamatsu, Y., Satomura, T., Kawakami, R., and Ohshima, T. (2001) Purification, characterization, and application of a novel dye-linked L-proline dehydrogenase from a hyperthermophilic archaeon, *Thermococcus profundus*, *Appl Environ Microbiol 67*, 1470-1475.
9. Kawakami, R., Sakuraba, H., and Ohshima, T. (2004) Gene and primary structures of dye-linked L-proline dehydrogenase from the hyperthermophilic archaeon *Thermococcus profundus* show the presence of a novel heterotetrameric amino acid dehydrogenase complex, *Extremophiles 8*, 99-108.
10. Kawakami, R., Sakuraba, H., Tsuge, H., Goda, S., Katunuma, N., and Ohshima, T. (2005) A second novel dye-linked L-proline dehydrogenase complex is present in the hyperthermophilic archaeon *Pyrococcus horikoshii* OT-3, *FEBS J 272*, 4044-4054.
11. Monaghan, P. J., Leys, D., and Scrutton, N. S. (2007) Mechanistic aspects and redox properties of hyperthermophilic L-proline dehydrogenase from *Pyrococcus furiosus* related to dimethylglycine dehydrogenase/oxidase, *FEBS J 274*, 2070-2087.
12. Tsuge, H., Kawakami, R., Sakuraba, H., Ago, H., Miyano, M., Aki, K., Katunuma, N., and Ohshima, T. (2005) Crystal structure of a novel FAD-, FMN-, and ATP-containing L-proline dehydrogenase complex from *Pyrococcus horikoshii*, *J Biol Chem 280*, 31045-31049.
13. Verhagen, M. F., Menon, A. L., Schut, G. J., and Adams, M. W. (2001) *Pyrococcus furiosus*: large-scale cultivation and enzyme purification, *Methods Enzymol 330*, 25-30.

14. Schut, G. J., Brehm, S. D., Datta, S., and Adams, M. W. (2003) Whole-genome DNA microarray analysis of a hyperthermophile and an archaeon: *Pyrococcus furiosus* grown on carbohydrates or peptides, *J Bacteriol 185*, 3935-3947.
15. Schut, G. J., Zhou, J., and Adams, M. W. (2001) DNA microarray analysis of the hyperthermophilic archaeon *Pyrococcus furiosus*: evidence for anNew type of sulfur-reducing enzyme complex, *J Bacteriol 183*, 7027-7036.
16. Dailey, H. A., Finnegan, M. G., and Johnson, M. K. (1994) Human ferrochelatase is an iron-sulfur protein, *Biochemistry 33*, 403-407.

Table 2.1. Specific activities of POR and PDH in extracts of *P. furiosus* cells grown under different conditions. [a]Specific activity is reported in μmoles methyl viologen reduced/min/mg for POR and μmoles DCIP reduced/min/mg for PDH.

Enzyme	Growth Condition	Specific Activity [a]
POR	Peptides/sulfur	3.48
	Maltose	4.5
	Maltose/sulfur	2.11
PDH	Peptides/sulfur	0.0238
	Maltose	0.0003
	Maltose/sulfur	0.0014

Table 2.2. Purification of PDH1 from *P. furiosus*. The different purification steps are, S100, the cell debris cleared supernatant, QHP, active fractions from the Q anion exchange column, Phenyl Sepharose, the active fractions from the hydrophobic interaction column, HAP, the active fractions from the hydroxyapatite column. [a]Specific activity is reported in μmoles DCIP reduced/min/mg.

nPDH1	Total Amount (mg)	Specific[a] Activity	Total Amount (U)	% Yield	Fold Purification
S100	547	0.024	12.6	100	1
QHP	22.2	0.15	3.2	25.8	2.9
Phenyl Sepharose	8.8	0.18	1.6	12.7	7.9
HAP	1	0.54	0.6	4.8	23.3

Table 2.3. Purification table of recombinant PDH1. The different purification steps are WCE, whole cell extract, S100, the cell debris cleared supernatant, Nickel, active fractions from the nickel column, and HAP, the active fractions from the hydroxyapatite column. [a]Specific activity is reported in μmoles DCIP reduced/min/mg.

rPDH1	Total Amount (mg)	Specific[a] Activity (U/mg)	Total Amount (U)	% Yield	Fold Purification
WCE	1036	0.037	37.92	100	1
S100	181	0.27	49.92	131	7
Nickel	54.6	0.77	42	110	21
HAP	44.3	0.91	40.32	106	24

Figure 2.1. Lanes are as follows: 1, cell debris cleared supernatant from peptide/sulfur grown cells, 2, pool of active fractions from QHP anion exchange column, 3, pool of active fractions from phenyl sepharose column, 4, pure PDH1 from hydroxyapatite column, 5, active fractions from rPDH1 nickel column elute, 6, active fractions from rPDH1 hydroxyapatite column.

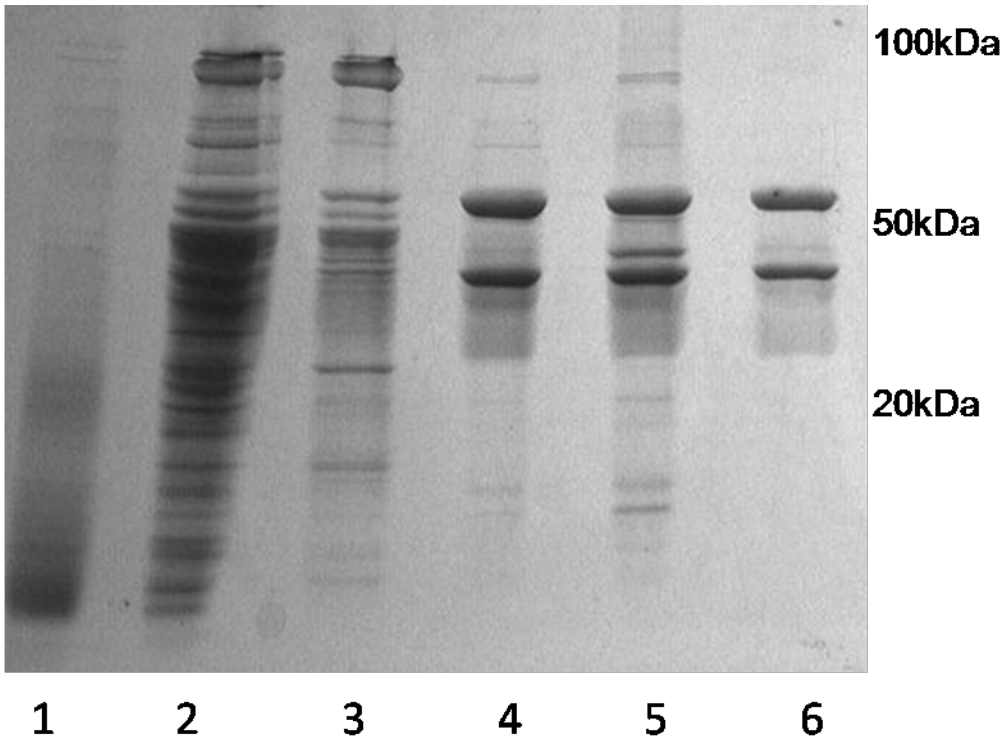
100kDa
50kDa
20kDa
1
2
3
4
5
6

Figure 2.2. EPR spectra of PDH1 reduced with 50mM Proline as a function of temperature. The spectra were recorded for samples of 0.24mM PDH1 with a microwave frequency of 9.603GHz, modulation amplitude of 0.65 millitesla, and a microwave power of 2 milliwatt.

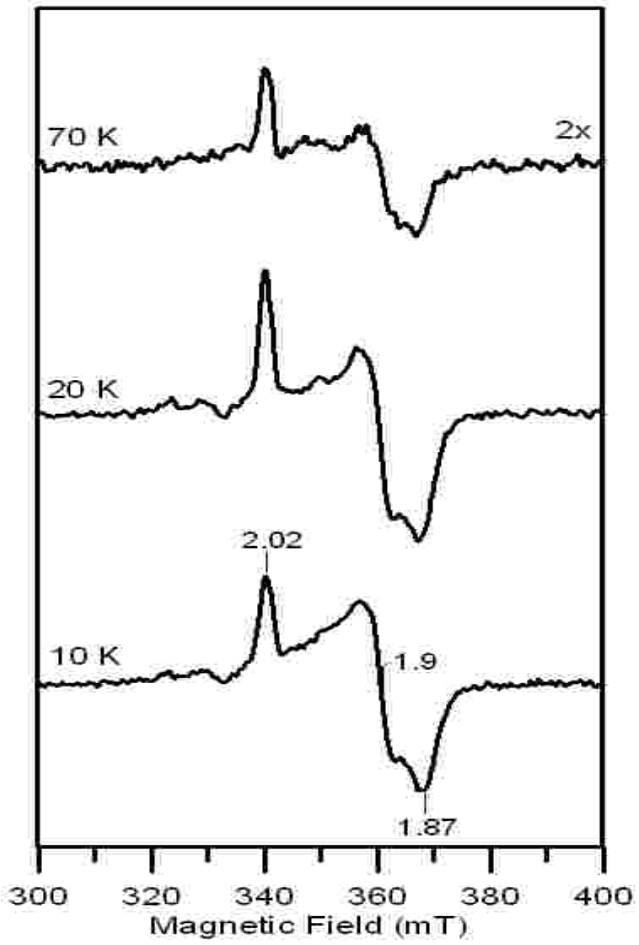
70 K
2x
20 K
2.02
10 K
1.9
1.87
300
320
340
360
380
400
Magnetic Field (mT)

Figure 2.3. EPR spectra of PDH1, as-purified and reduced with 2mM Dithionite and 50mM Proline (top to bottom). The spectra were recorded for samples of 0.24mM PDH1 at 10K with a microwave frequency of 9.603GHz, modulation amplitude of 0.65 millitesla, and a microwave power of 20 milliwatt.

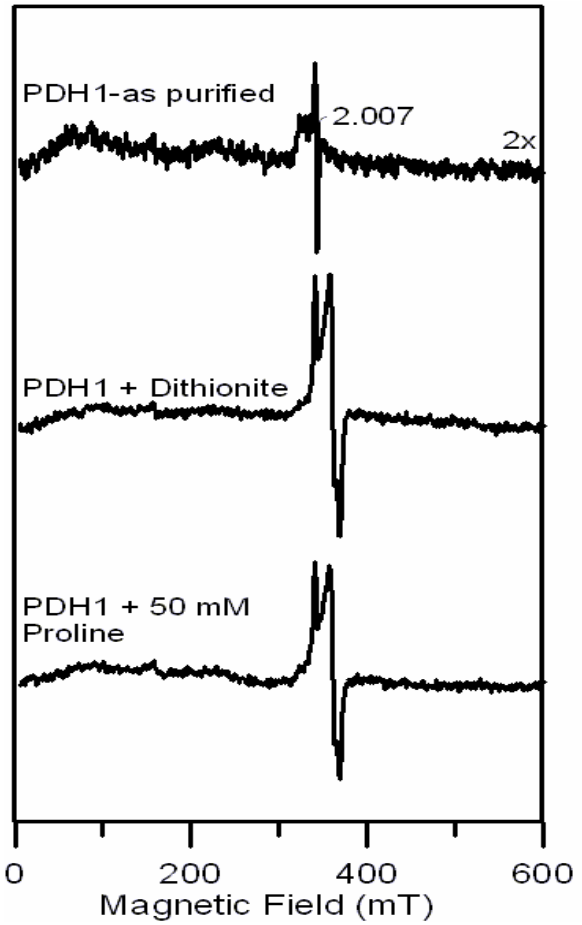
PDH1-as purified
2.007
2x
PDH1 + Dithionite
PDH1 + 50 mM
Proline
0
200
400
600
Magnetic Field (mT)

Table 2.4. Properties of PDH1 with and without an iron-sulfur cluster. There was no data for the enzyme without the cluster towards resorufin as the activity did not exist.

	2,6 - Dichloroindophenol		Resorufin		
Assay Temp.	50°C	50°C	50°C	50°C	80°C
[2Fe-2S]	(-)	(+)	(-)	(+)	(+)
Specific Activity	1.8 µmoles/min/mg	2.1 µmoles/min/mg	n/d	0.028 µmoles/min/mg	0.094 µmoles/min/mg
K_m	4200 ± 168µM	3800 ± 38µM	n/d	27.9 ± 1.7µM	87.3 ± 1.7µM

Figure 2.4. Proposed electron pathway through PDH1. The pathway for electron flow through the cluster is indicated by the dashed lines.

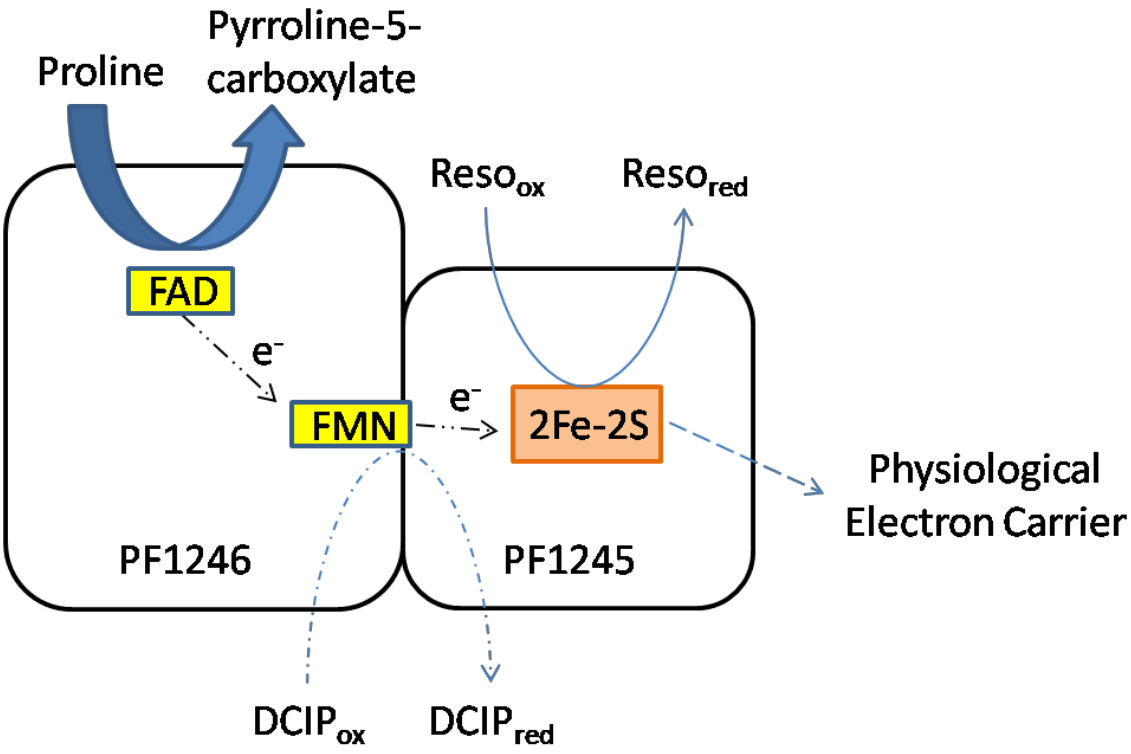
Proline
Pyrroline-5-carboxylate
Reso$_{ox}$
Reso$_{red}$
FAD
e$^-$
FMN
e$^-$
2Fe-2S
Physiological Electron Carrier
PF1246
PF1245
DCIP$_{ox}$
DCIP$_{red}$

REFERENCES

1. Scarpulla, R. C., and Soffer, R. L. (1978) Membrane-bound proline dehydrogenase from *Escherichia coli*. Solubilization, purification, and characterization, *J Biol Chem 253*, 5997-6001.
2. Menzel, R., and Roth, J. (1981) Purification of the putA gene product. A bifunctional membrane-bound protein from *Salmonella typhimurium* responsible for the two-step oxidation of proline to glutamate, *J Biol Chem 256*, 9755-9761.
3. Menzel, R., and Roth, J. (1981) Regulation of the genes for proline utilization in *Salmonella typhimurium*: autogenous repression by the putA gene product, *J Mol Biol 148*, 21-44.
4. Gu, D., Zhou, Y., Kallhoff, V., Baban, B., Tanner, J. J., and Becker, D. F. (2004) Identification and characterization of the DNA-binding domain of the multifunctional PutA flavoenzyme, *J Biol Chem 279*, 31171-31176.
5. Lee, Y. H., Nadaraia, S., Gu, D., Becker, D. F., and Tanner, J. J. (2003) Structure of the proline dehydrogenase domain of the multifunctional PutA flavoprotein, *Nat Struct Biol 10*, 109-114.
6. Wood, J. M. (1987) Membrane association of proline dehydrogenase in *Escherichia coli* is redox dependent, *Proc Natl Acad Sci U S A 84*, 373-377.
7. Muro-Pastor, A. M., Ostrovsky, P., and Maloy, S. (1997) Regulation of gene expression by repressor localization: biochemical evidence that membrane and DNA binding by the PutA protein are mutually exclusive, *J Bacteriol 179*, 2788-2791.
8. Sakuraba, H., Takamatsu, Y., Satomura, T., Kawakami, R., and Ohshima, T. (2001) Purification, characterization, and application of a novel dye-linked L-proline dehydrogenase from a hyperthermophilic archaeon, *Thermococcus profundus*, *Appl Environ Microbiol 67*, 1470-1475.
9. Kawakami, R., Sakuraba, H., and Ohshima, T. (2004) Gene and primary structures of dye-linked L-proline dehydrogenase from the hyperthermophilic archaeon *Thermococcus profundus* show the presence of a novel heterotetrameric amino acid dehydrogenase complex, *Extremophiles 8*, 99-108.
10. Kawakami, R., Sakuraba, H., Tsuge, H., Goda, S., Katunuma, N., and Ohshima, T. (2005) A second novel dye-linked L-proline dehydrogenase complex is present in the hyperthermophilic archaeon *Pyrococcus horikoshii* OT-3, *FEBS J 272*, 4044-4054.
11. Monaghan, P. J., Leys, D., and Scrutton, N. S. (2007) Mechanistic aspects and redox properties of hyperthermophilic L-proline dehydrogenase from *Pyrococcus furiosus* related to dimethylglycine dehydrogenase/oxidase, *FEBS J 274*, 2070-2087.
12. Tsuge, H., Kawakami, R., Sakuraba, H., Ago, H., Miyano, M., Aki, K., Katunuma, N., and Ohshima, T. (2005) Crystal structure of a novel FAD-, FMN-, and ATP-containing L-proline dehydrogenase complex from *Pyrococcus horikoshii*, *J Biol Chem 280*, 31045-31049.
13. Verhagen, M. F., Menon, A. L., Schut, G. J., and Adams, M. W. (2001) *Pyrococcus furiosus*: large-scale cultivation and enzyme purification, *Methods Enzymol 330*, 25-30.

14. Schut, G. J., Brehm, S. D., Datta, S., and Adams, M. W. (2003) Whole-genome DNA microarray analysis of a hyperthermophile and an archaeon: *Pyrococcus furiosus* grown on carbohydrates or peptides, *J Bacteriol 185*, 3935-3947.
15. Schut, G. J., Zhou, J., and Adams, M. W. (2001) DNA microarray analysis of the hyperthermophilic archaeon *Pyrococcus furiosus*: evidence for anNew type of sulfur-reducing enzyme complex, *J Bacteriol 183*, 7027-7036.
16. Dailey, H. A., Finnegan, M. G., and Johnson, M. K. (1994) Human ferrochelatase is an iron-sulfur protein, *Biochemistry 33*, 403-407.

CHAPTER 3

AN AUTOMATED, HIGH-THROUGHPUT SYSTEM FOR ANAEROBIC CRYSTALLIZATION OF OXYGEN SENSITIVE COFACTOR CONTAINING PROTEINS IMPLEMENTED IN THE X-RAY STRUCTURE SOLUTION OF RUBRERYTHRIN[1]

[1]Bret Donald Dillard, M. W. W. Adams, John Rose and Bi-Cheng Wang (To be submitted to *AKTA D*)

Abstract

The ability to crystallize proteins and study their structure/function relationship sometimes relies on the capability to reproduce the environment in which the proteins are naturally active. When working with enzymes purified from organisms that are obligate anaerobes one must often use an anaerobic environment in order to maintain oxygen sensitive cofactors such as metal centers that are present in many proteins as they exist in the native cytoplasm. We have developed a system that reproduces that environment and allows for the determination of biologically relevant structures of macromolecules in a high throughput fashion. The automated crystallization system that has been developed can carry out microbatch and vapor diffusion experiments in a completely anaerobic environment. The system has been validated by determining the x-ray structure solution of the oxygen-sensitive enzyme rubrerythrin from the hyperthermophilic archaeon, *Pyrococcus furiosus.* The structure of the enzyme is compared with its mesophilic counterpart from *Desulfovibrio vulgaris*.

Introduction

Crystallization of enzymes containing oxygen-sensitive cofactors is an expensive (in terms of protein) and time-consuming process. Typically, one would carry out capillary or vapor batch crystallization experiments, which require excessive protein and labor. The capillary experiments require 10 to 30µl of protein which is usually at a concentration of 5 to 25mg/ml while vapor batch experiments require as little as 0.5µl but the mother liquor must be considered, which is usually 200µl to 500µl and each condition must be anoxic as well[1, 2]. Using a Douglas Instruments Oryx 1-6 crystallization robot placed inside of an Bactron X anaerobic chamber altered to allow electronic communication across the chamber barrier we have created a system which uses as little as 200 nl of protein and requires that crystallization solutions be degassed only once in order to carry out 400 individual experiments when each well contains a total of 1µl whereas the other two methods mentioned will require much more volume of each crystallization condition and protein per experiment.

To validate the system, the iron-containing rubrerythrin from *Pyrococcus furiosus* was chosen as a test case. This enzyme is involved in the removal of reactive oxygen species in an obligately anaerobic organism[3]. It functions as a rubredoxin-dependent peroxidase that catalyzes the conversion of hydrogen peroxide to water [3]. The X-ray crystal structure of this enzyme was previously solved by the structural genomics effort at the Southeast Collaboratory for Structural Genomics (SECSG) using the zinc substituted form that is stable in oxygen. The structure has been deposited in the Protein Data Bank as 1NNQ[4]. The entire experiment for the solution of the structure of the oxygen-stable enzyme was carried out in an aerobic environment [4]. It was previously shown that the native enzyme contained 3 iron atoms per monomer and precipitated

upon exposure to oxygen[3]. Metal analysis on the recombinant form, which was used for crystallization, showed that a mixture of iron, cobalt, and zinc were present and that there was only a total of 1 metal atom per monomer with zinc being the predominate metal (0.60 atoms/mole). Presumably the metals were mostly coordinated in the mononuclear iron site as that site had occupancy of 0.90 in the crystal structure [4]. The occupancy of the metal atoms at the di-iron site in the structure was reduced to 0.20 in order to correct for excessive electrons attributed to zinc in the density when a difference map was calculated[4]. The structure was shown to be a dimer and the enzyme also showed an interesting feature of domain swapping where two helices of the four helix bundle were swapped from one polypeptide with that from the other[4]. The native, iron-only enzyme crystallized by modified microbatch in the anaerobic chamber using the Douglas robot. The structure was determined to 2.4Å resolution using data recorded using a MAR 300 charge-coupled device (CCD) detector and 1.54Å synchrotron X-rays (beamline 22-ID Advanced Photon Source, Argonne National Laboratory). All six iron atoms for the dimer were found by Patterson analysis and were used for single wavelength anomalous dispersion (SAD) phasing of the measured structure factors.

Materials and methods

Anaerobic chamber: A Bactron X Chamber was purchased from Sheldon Manufacturing Inc. This system was chosen because the chamber wall could be modified to allow electronic communication between the computer outside the chamber (Fig. 3.11) and the MCC for the robot inside the chamber. The chamber is fitted with a dual gas system that allows for flushing of the antechamber with nitrogen multiple times to remove oxygen and then a final cycle of 95% nitrogen/ 5% hydrogen. This chamber utilizes a palladium catalyst to generate water by reducing

any oxygen that may enter with hydrogen (Fig. 3.2). The system is capable of maintaining total the oxygen content below 1ppm, as measured by an oxygen detector (Coy Laboratory Products Inc.), excepting times when samples and other materials are placed into the chamber where the oxygen content typically increases to 100ppm oxygen. However, the oxygen content is quickly reduced to 1ppm by oxygen removal by the catalyst.

Crystallization robot and preparation of crystallization conditions

An Oryx 1-6 robot from Douglas Instruments was placed in the chamber, which allowed about 3 inches clearance from the front of the chamber when the plate loader was fully extended. All water used to maintain hydraulic pressure in the dispensing tubes was degassed by multiple cycles of vacuum and positive pressure argon (see below) prior to being loaded into the robot. Standard programs for screening using modified microbatch designed by Douglas Instruments were used in carrying out all experiments. Crystallization screening kits were purchased from Hampton Research. Exactly 200µl of each condition was transferred to a 0.5 dram vial and sealed with a stopper. Each condition was then placed under a vacuum of 30 inches Hg for 5 minutes and then purged with argon until positive pressure was reached. This procedure was repeated 5 times for each condition in order to remove any oxygen present. Once each condition was made anoxic it was placed in the chamber and transferred to a 96-well polypropylene plate and covered with 100% paraffin oil that had been previously degassed.

Purification, crystallization, mounting, data collection, and structure solution of native *Pyrococcus furiosus* rubrerythrin.

The enzyme was purified as previously described except that 500g of cells were broken and the protocol was adjusted for the larger amount of protein present. Importantly, all manipulations were carried out under strictly anaerobic conditions[3]. Purity was checked by

SDS-PAGE analysis and the protein was concentrated to 19.6mg/ml in 50 mM BisTris, pH 7.0, 200 mM NaCl buffer and introduced into the chamber. The Oryx 1-6 was then used to set up the crystallization screen using 1 µl drops containing equal volumes of protein concentrate and precipitant cocktail. All plates were covered with 4ml of 80:20 mixture of paraffin and silicon oils. The protein crystallized in 20% (w/v) PEG-3000, 0.1M Tris, pH 7.0 and precipitant. A single crystal was harvested with a cryoloop (Hampton Research, HR4-747) and briefly immersed in a 1 µl drop containing a 1:4 mixture of glycerol and the precipitant solution prior to being flash-frozen and stored in liquid nitrogen. Data were collected at 22-ID Advanced Photon Source, Argonne National Laboratory using a MAR 300 CCD detector and 1.54 Å X-rays and 360° were collected at 1° intervals. The data was indexed, integrated, and scaled using HKL2000[5]. Six iron atoms were located by Patterson map analysis using XPREP and the structure factors were phased by the ISAS method running with SGXPRO [6, 7]. The initial model was built using Arp/Warp from the CCP4 program suite[8]. Multiple cycles of model building in COOT followed by refinement with Refmac from the CCP4 program suite completed the structure solution with R_{work} = 17.6% and R_{free} = 20.4% [8, 9]. The solution was analyzed using the program MolProbity and scored in the 99th percentile for structures of this resolution[10].

Results and Discussion

Anaerobic crystallography: A system was constructed for the efficient screening for crystallization conditions of proteins that contain oxygen-sensitive cofactors. While it is important to have a structure of the native enzyme from *Pyrococcus furiosus*, in this communication we describe the construction of a system that carries out the efficient crystallization of proteins containing oxygen-sensitive cofactors. The Oryx 1-6 robot designed by Douglas Instruments is capable of dispensing a 96 well screen in less than 30 minutes using

48µl of protein considering a 1µl total drop size. We feel that the most effective aspect of this system is that the crystallization conditions are available immediately to be dispensed a second time. Each well on the source plate contains 200µl of crystallization condition that allows for 400 separate experiments at 1µl total volume to be conducted from one set of degassed solutions whereas other methods require either larger volume or multiple samples to be degassed.

The system has been validated by the solution of the oxygen sensitive protein rubrerythrin from *Pyrococcus furiosus*. The system was maintained under anaerobic conditions throughout the entire experiment. Using the Douglas robot inside the chamber the crystallization screens produced 26 crystallization hits, which were tested for diffraction quality prior to selection of the crystal used for data collection. The crystal that was chosen belonged to space group $P4_22_12$ and had unit cell parameters of a = b = 105.73, c = 80.32. The data set was 95.59% complete with an internal agreement (R_{sym}) of 10.0% and a redundancy of 13.1 for the resolution range 19.07 - 2.41Å. Assuming two molecules in the asymmetric unit, all six iron atoms were found by Patterson analysis as illustrated in figure 3.4. The data set was collected using 1.54Å x-rays so there would be no anomalous signal for zinc if it were present. However, metal analysis of the native enzyme showed no zinc was present in relevant amounts[3]. The occupancies of the metal sites in 1NNQ were lowered in order to correct for excess electrons when a difference map was calculated.

The structure of the rubrerythrin from *D. vulgaris* (PDB code: 1LKO) has been determined and contains two water molecules that are involved in stabilizing the diiron active site and these can be easily seen in the structure of the native *P. furiosus* protein, while they are not present in the structure solved with zinc[11]. Upon comparison of the structures of the *P. furiosus* and *D. vulgaris* enzymes, the most striking difference is the domain swapping [4]. The Cα

r.m.s.d. value calculated using only the four helix bundles from each structure is 0.823Å. The active site residues of the di-iron site give an all atom r.m.s.d. of 0.631Å where the active site residues are defined as all atoms of a residue that have one atom within 5Å of one of the iron atoms.

When the overall folds of rubrerythrin from *P. furiosus* and *D. vulgaris* are compared the most striking difference is the domain swapping feature. The domain swapping feature is distinct among structures of the rubrerythrin family from thermophilic organisms as the x-ray crystal structures of mesophilic forms DvRbr and DvNgr do not show this feature. We hypothesize that it is this feature that contributes to the thermal stability of the enzyme. Upon comparison of the features typically attributed to thermal stability such as salt bridges and hydrogen bonding, the difference between the thermophilic and mesophilic structures is very small and there are actually a larger number of the stabilizing features in the mesophilic form. The mesophilic rubrerythrin contains 374 hydrogen bonds and 40 salt bridges, the mesophilic nigerythrin structure contains 421 hydrogen bonds and 32 salt bridges, and the hyperthermophilic rubrerythrin contains 341 hydrogen bonds and 21 salt bridges. The hydrogen bonds were calculated by all non-water interactions using the program Chimera and the salt bridges were calculated using the program ESBRI [12, 13].

When protein-protein interactions are considered as a factor in increasing thermal stability, the thermophilic forms of the rubrerythrin family contain many more interactions due to the domain swapping feature. The domain swapping feature increases almost all protein-protein interactions, but the largest difference between the mesophilic is when hydrophobic interactions are considered. When the hydrophobic interactions due to protein-protein interfaces are considered between PfRbr and DvRbr, PfRbr has 4.5 times as many (Table 2)[14]. This is a direct

consequence of the domain swapping feature. When the thermophilic sulerythrin is compared with DvRbr, even with its shorter peptide length, it contains 3.1 times as many hydrophobic interactions. While there are also increased side chain hydrogen bonds and pi-interactions of inter-protein interactions in the thermophilic structures, the increased hydrophobic interactions appear to be the main contributing factor to protein thermal stability.

Another aspect that distinguishes the meso- and thermophilic forms of this enzyme is how domain swapping leads to a more compact structure that eliminates a hole that exists in the mesophilic form which allows for more of the surface of the enzyme to be solvated, which in turn contributes to the lower number of hydrophobic interactions. Recently it was shown that extreme thermophiles display significant trends among their protein structures towards becoming more "ball-like"[15]. In this work the authors developed two terms, travel depth and burial depth. Travel depth is the distance from the convex hull to the molecular surface that avoids the protein interior and burial depth is distance from the molecular surface to each atom. These definitions allow one to distinguish between thermophilic and mesophilic structures of homologous proteins by indicating smaller, less numerous and less deep pockets in thermophilic structures and that thermophilic proteins bury more surface area and are more compact. The mesophilic structure has a volume and surface area of 46,940$Å^3$ and 16,800$Å^2$ whereas the thermophilic structure has a volume and surface area of 42,890$Å^3$ and 13,760 $Å^2$ and upon visual inspection of the surface of the structures the thermophilic form has smaller and less deep pockets than its mesophilic counterpart.

Acknowledgements

This work was supported in part with funds from the National Institutes of Health (GM62407), The Georgia Research Alliance and the University of Georgia Research Foundation. Data were collected at Southeast Regional Collaborative Access Team (SER-CAT) 22-ID beamline at the Advanced Photon Source, Argonne National Laboratory. Supporting institutions may be found at www.ser-cat.org/members.html. Use of the Advanced Photon Source was supported by the U. S. Department of Energy, Office of Science, Office of Basic Energy Services, under Contract No. W-31-109-Eng-38.

Table 3.1. Data collection and refinement statistics for reduced *P.furiosus* rubrerythrin.

Table 1. Data collection parameters and statistics for PfRbr

X-ray source	APS22ID
Detector	MAR300 CCD
Wavelength (Å)	1.54
Oscillation width (°)	1°
No. of images	360
Resolution (Å)	19.0-2.4 (2.47-2.4)
Unit-cell parameters	α=β=γ=90°
a = b (Å)	105.7
c (Å)	80.3
Space group	$P4_22_12$
Redundancy	13.9
Unique reflections	12,220
Completeness (%)	95.6 (83.9)
I/Sigma(I)	26.1 (3.1)
Rsym (%)	8.3 (26.8)

Table 3.2. Comparison of stabilizing protein-protein interactions in *P. furiosus* rubrerythrin. The largest difference between the mesophilic and (hyper)thermophilic forms are hydrophobic interactions. The total inter-protein interactions are also much greater in the thermophilic forms when compared to the mesophilic forms. Interactions were calculated using the Protein Interactions Calculator (http://crick.mbu.iisc.ernet.in/~PIC/).

	Meso		Therm	Hypertherm
	DvNgr	DvRbr	StSlr	PfRbr
Protein-Protein Hydrophobic Interactions	14	20	62	91
Protein-Protein Main Chain-Side Chain Hydrogen Bonds	22	28	14	30
Protein-Protein Side Chain-Side Chain Hydrogen Bonds	42	38	64	48
Protein-Protein Ionic Interactions	8	6	8	8
Protein-Protein Cation-Pi Interactions	2	4	6	10
Total Protein-Protein Interactions	88	96	154	187

Figure 3.1. Parallel port in chamber wall that allows for electronic communication between the robot and computer.

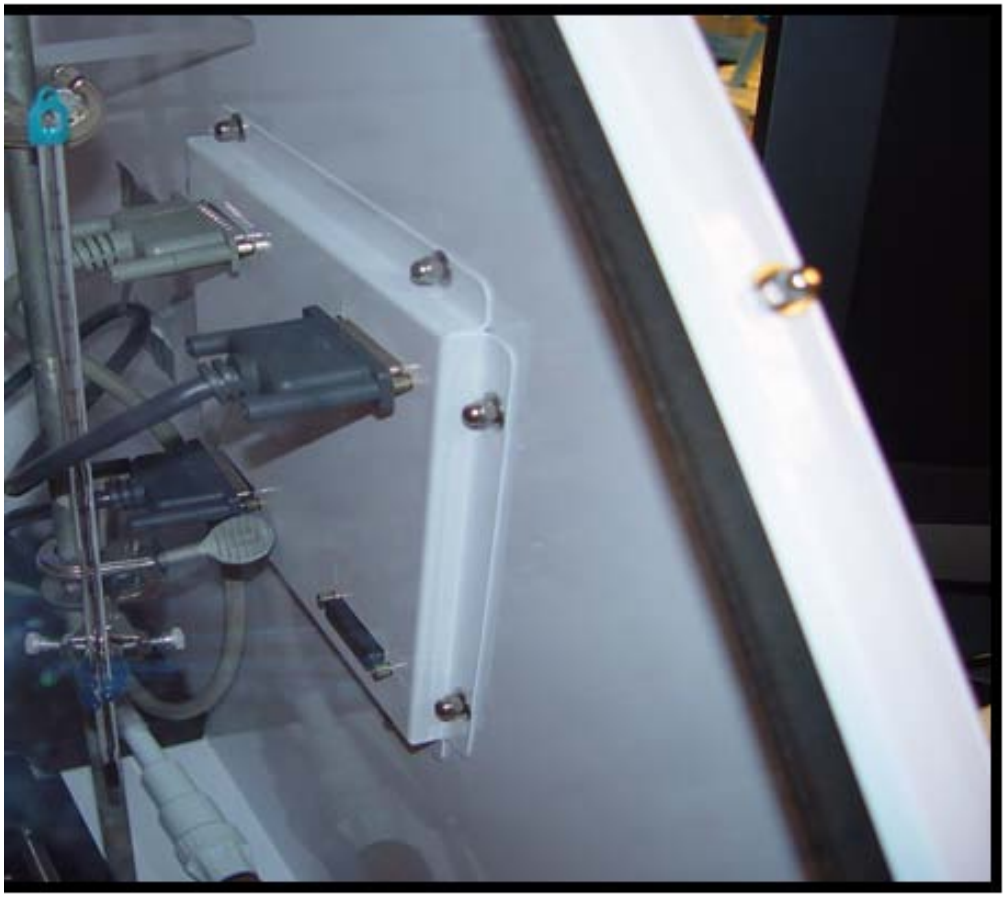

Figure 3.2. Palladium catalyst (top left) and oxygen sensor are used for the detection and removal of oxygen.


OXYGEN
PPM
HYDROGEN
%
000
02.6
HI
LO
OFF
ON
POWER
ALARM CONTROL
ALARM SET
COY LABORATORY PRODUCTS INC.
WARNING
NOT SUITABLE TO MONITOR ADDITION OF PURE HYDROGEN. USE ONLY PRE-MIXED GASES. (SEE OPERATOR MANUAL)

Figure 3.3. Patterson map calculated from the scaled data showing positions of the iron atoms.

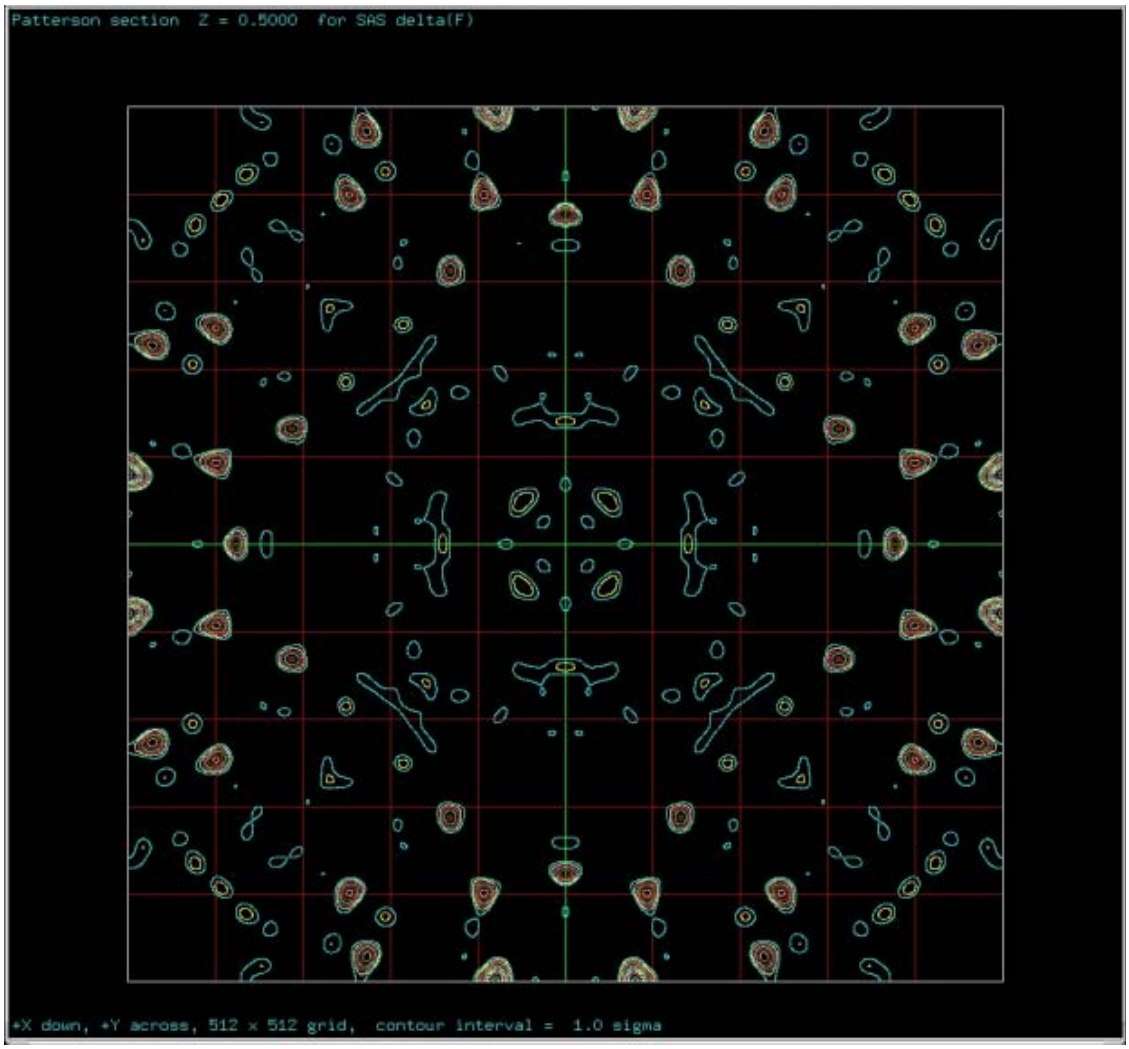
Patterson section Z = 0.5000 for SAS delta(F)
+X down, +Y across, 512 × 512 grid, contour interval = 1.0 sigma

References

1 Drenth J, Hol WG, Wierenga RK. Crystallization and preliminary x-ray investigation of p-hydroxybenzoate hydroxylase from Pseudomonas fluorescens. J Biol Chem 1975, 250: 5268-5269

2 Hsieh YC, Liu MY, Le Gall J, Chen CJ. Anaerobic purification and crystallization to improve the crystal quality: ferredoxin II from Desulfovibrio gigas. Acta Crystallogr D Biol Crystallogr 2005, 61: 780-783

3 Weinberg MV, Jenney FE, Jr., Cui X, Adams MW. Rubrerythrin from the hyperthermophilic archaeon Pyrococcus furiosus is a rubredoxin-dependent, iron-containing peroxidase. J Bacteriol 2004, 186: 7888-7895

4 Tempel W, Liu ZJ, Schubot FD, Shah A, Weinberg MV, Jenney FE, Jr., Arendall WB, 3rd, *et al.* Structural genomics of Pyrococcus furiosus: X-ray crystallography reveals 3D domain swapping in rubrerythrin. Proteins 2004, 57: 878-882

5 Otwinowski Z MW. Processing of X-ray diffraction data collected in oscillation mode. . Methods Enzymol (1997): 307-326

6 McRee DE. XtalView/Xfit--A versatile program for manipulating atomic coordinates and electron density. J Struct Biol 1999, 125: 156-165

7 Fu ZQ, Rose J, Wang BC. SGXPro: a parallel workflow engine enabling optimization of program performance and automation of structure determination. Acta Crystallogr D Biol Crystallogr 2005, 61: 951-959

8 The CCP4 suite: programs for protein crystallography. Acta Crystallogr D Biol Crystallogr 1994, 50: 760-763

9 Emsley P, Cowtan K. Coot: model-building tools for molecular graphics. Acta Crystallogr D Biol Crystallogr 2004, 60: 2126-2132

10 Davis IW, Murray LW, Richardson JS, Richardson DC. MOLPROBITY: structure validation and all-atom contact analysis for nucleic acids and their complexes. Nucleic Acids Res 2004, 32: W615-619

11 deMare F, Kurtz DM, Jr., Nordlund P. The structure of Desulfovibrio vulgaris rubrerythrin reveals a unique combination of rubredoxin-like FeS4 and ferritin-like diiron domains. Nat Struct Biol 1996, 3: 539-546

12 Pettersen EF, Goddard TD, Huang CC, Couch GS, Greenblatt DM, Meng EC, Ferrin TE. UCSF Chimera--a visualization system for exploratory research and analysis. J Comput Chem 2004, 25: 1605-1612

13 Costantini S, Colonna G, Facchiano AM. ESBRI: A web server for evaluating salt bridges in proteins. Bioinformation 2008, 3: 137-138

14 Tina KG, Bhadra R, Srinivasan N. PIC: Protein Interactions Calculator. Nucleic Acids Res 2007, 35: W473-476

15 Coleman RC. Thermophilic protein structure adaptation examined with Burial Depth and Travel Depth Biophys J 2009, 96: 584a

CHAPTER 4

NEW INSIGHTS INTO THE MECHANISM OF NON-HEME PEROXIDASES BY TRAPPING INTERMEDIATES IN RUBRERYTHRIN FROM *PYROCOCCUS FURIOSUS*[1]

[1]Bret D. Dillard, Michael W. W. Adams and William N. Lanzilotta (Submitted to *The Journal of Biological Inorganic Chemistry*)

SUMMARY

Anaerobically prepared, fully reduced (all ferrous) crystals of rubrerythrin from *Pyrococcus furiosus* (PfRbr) were treated with H_2O_2 in a time dependent manner before being rapidly frozen in an anaerobic chamber at 23°C. At this temperature the enzyme is in a cryogenic state and retains only 1-2 % of the activity observed at the physiological temperature (100°C). Subsequent analysis of these crystals by X-ray diffraction revealed a rapid deterioration in the overall diffraction quality and resolution, consistent with the observation of enzyme precipitation upon oxidation *in vitro*. However, crystals that were frozen within ten seconds of peroxide treatment diffracted to 2.0 angstroms and allowed for further data collection. Herein we present evidence for new intermediates in the reaction mechanism of peroxide reduction. Furthermore, a structural explanation is provided for the redox-dependent change in solubility observed for PfRbr. Specifically, these results provide evidence for a peroxy intermediate and further confirm that the characteristic combination of iron sites together with redox-dependent iron-toggling accounts for the selectivity for hydrogen peroxide over dioxygen by rubrerythrin.

INTRODUCTION

A number of enzymes in both bacteria and higher organisms function specifically to remove reactive oxygen species (ROS) that are formed as a result of metabolic processes or diffusion of molecular oxygen into cells that is then adventitiously reduced at the active sites of redox enzymes containing flavins or quinones [1]. While the detoxification of ROS by the superoxide dismutase (SOD)/catalase system is prevalent in aerobic microorganisms, this system is missing in most anaerobes [2-4]. For strictly anaerobic organisms, the generation of molecular oxygen by the SOD system would have a deleterious effect. Consequently, most strictly anaerobic organisms contain superoxide reductase (SOR), which reduces rather than dismutates superoxide to peroxide, and therefore O_2 is not generated [2, 5, 6]. Recent observations strongly indicate that the physiological function of the peroxidase-dependent SOR system is to quickly and efficiently remove O_2 and H_2O_2 [2, 7, 8].

For the SOR system, substantial *in vivo* [5, 9, 10] and *in vitro* [6-8, 11] observations strongly supports the proposal that the enzyme rubrerythrin (Rbr) functions as the terminal component of a rubredoxin-(Rub)-dependent peroxidase as where NAD(P)H is the ultimate electron source via a NADH rubredoxin oxidoreductase (NROR), outlined in Reactions 1 and 2.

NROR/Rd/Rbr: $NAD(P)H + H^+ + H_2O_2 \xrightarrow{\text{NAD(P)H:Rbr oxidoreductase + Rbr}} NAD(P) + 2H_2O$ (1) Rd/Rbr:

$2H^+ + 2Rub(Fe^{+2}) + H_2O_2 \xrightarrow{\text{Rbr}} 2Rub(Fe^{+3}) + 2H_2O$ (2)

Rubrerythrins are characterized by the unique combination of two common domains, each containing a metal center. The larger domain is comprised of a hemerythrin-like four helix bundle that contains a non-sulfur, oxo-bridged diiron site that is similar to that found in ferritin

or methane monooxygenase. The second smaller rubredoxin-like domain contains a single [$Fe(SCys)_4$] center. When the "classical" rubrerythrins were initially characterized, it was discovered that the hemerythrin-like fold was the N-terminal domain while the rubredoxin domain was found near the C-terminus. More recently, and in direct response to oxidative stress, the reverse rubrerythrins have been characterized and are so termed because the order of these two domains within the gene product is reversed [2, 12]. Several lines of evidence have shown that the reactivity of Rbr towards oxygen is low compared to that of peroxide and that during peroxide reduction the diiron site serves to directly reduce peroxide to water while the [$Fe(SCys)_4$] site transfers electrons from an exogenous electron donor to the oxidized diiron site following peroxide reduction [2]. A general reaction mechanism for the homologous protein, nigerythrin (from *Desulfovibrio vulgaris,* DvNgr) is depicted in Figure 1 but can be inferred for all rubrerythrins.

The proposed mechanism for Rbr-catalyzed hydrogen peroxide reduction (Figure 1) is based largely on the crystal structures of fully oxidized (all-ferric), fully reduced (all-ferrous) DvRbr and DvNgr, as well as a μ-1,3 azido adduct of the all ferrous form of DvRbr [13-18]. Interestingly, DvNgr, which is similar to DvRbr in structure and function [5, 8, 19, 20], has a significantly higher peroxidase activity [8] and does not show the apparently artifactual ferroxidase activity displayed by DvRbr [21]. Direct reduction of H_2O_2 to water at the diiron site would certainly be advantageous in a strictly anaerobic organism and has been proposed to occur via a μ-1,2-H_2O_2 diferrous intermediate (Figure 1). The resulting oxo-bridged diferric site is subsequently re-reduced via two sequential intramolecular one-electron transfer events from the [$Fe(SCys)_4$] site in the rubredoxin domain to the diferric and mixed-valent [Fe(II),Fe(III)] diiron sites, respectively. An explanation for the greater turnover numbers observed for DvNgr

stemmed from the identification of a shorter and potentially more efficient electron transfer pathway from the rubredoxin iron to the diiron site [16]. In total these crystallographic data and ENDOR studies have demonstrated that the diiron site of rubrerythrins is very dynamic with one of the iron atoms moving more than 2Å upon conversion of the all-ferrous state to the mixed valance state [22-24]. Spectroscopic analyses unequivocally identified the diiron bridging solvent ligand as oxo in the all-ferric DvRbr [22, 23]. Moreover, ENDOR studies and the magnitude of antiferromagnetic coupling between the iron atoms [24] is consistent with a bridging hydroxo in place of oxo in the mixed-valent diiron site with the ferrous oxidation state localized on the His131-ligated iron. As a note keeping measure, the solvent exchange reaction is shown in Figure 1 by depicting the oxygen atoms derived from peroxide as filled in black.

In contrast to the work described above with enzymes from mesophilic organisms, studies with Rbrs from thermophilic organisms have been significantly less clear. For example, a recombinant, zinc-substituted Rbr from *Pyrococcus furiosus* (PfRbr), has been reported [25]. The observation of adventitiously bound zinc in a recombinant enzyme is consistent with additional reports demonstrating that care must be taken in order to avoid physiologically irrelevant metal exchange during isolation and crystallization [17]. However, in comparison to the structures of mesophilic rubrerythrins, a major difference observed in the PfRbr structure was the domain-swapped four-helix bundles [25]. The *in vivo* relevance of this is uncertain since the same protein purified directly from *P. furiosus* contains predominantly iron [6, 25]. Recently, the structure of "sulerythrin" from the strictly aerobic, thermoacidophilic archaeon *Sulfolobus todokaii* has also been solved and it also displays the domain-swapping feature. However, this enzyme does not contain the rubredoxin-like domain, nor is it oxygen-sensitive or have a measureable peroxidase activity [26, 27]. While these results suggest that domain swapping is

a common feature for Rbr stabilization at higher temperatures, it is clear that for PfRbr the iron-only form of the enzyme is the functional form and maximum activity is obtained at the physiological temperature of 100°C [6].

Subsequent anaerobic crystallization and structure determination of native iron-containing PfRbr has revealed a model identical to the recombinant structure which has zinc in place of the iron atoms (John Rose, personal communication, PDB ID codes 2HR5 and 1NNQ). While this is consistent with what has been observed for the fully reduced (all ferrous) DvRbr and DvNgr, whether or not archaeal enzymes and the PfRbr undergo the redox-dependent movement has not been determined. The underlying reason for this stems from the observation that upon chemical or substrate catalyzed oxidation of PfRbr, the enzyme becomes insoluble and rapidly precipitates [11]. This phenomenon occurs at 100 °C regardless of whether the oxidation has occurred as a result of peroxide reduction under anaerobic conditions or by the addition of an oxidant. It is interesting to note that the oxidation and accompanying change in solubility is completely reversible. Precipitated Rbr can be solubilized by resuspending it under anoxic conditions and adding a strong chemical reductant such as sodium dithionite (**Supplemental Movie 1**). Since the precipitation is accompanied by a color change from colorless to dark red, it is clear that the enzyme, and the rubredoxin site in particular, is in an all-ferric state when the enzyme begins to come out of solution.

In order to address whether or not the redox-dependent iron-toggling occurs in the archaeal rubrerythrin and further advance our understanding of the terminal peroxidase in the SOR system for strict anaerobes, as well as to provide an atomic explanation for the observed biochemical properties of the PfRbr, our goal was to capture intermediate states in the catalytic cycle following exposure of the PfRbr to H_2O_2. Since PfRbr is virtually inactive at room

temperature [11], we reasoned that under strictly anaerobic conditions, crystals of the fully reduced (all ferrous) enzyme could be treated with H_2O_2 (at 23°C) and rapidly frozen in order to trap potential intermediates in the reduction of peroxide. In this work we report the observation of two new intermediates in the non-heme peroxidase cycle and further provide an explanation for the redox-dependent change in the solubility of PfRbr.

RESULTS

Purification and crystallization of the native rubrerythrin from P. furiosus (PfRbr). PfRbr was isolated from *P. furiosus* cells that had been grown on maltose as previously reported [11]. Care was taken to insure that the enzyme remained in the reduced state so that oxidation resulting in precipitation did not occur. Since precipitation is not conducive to crystallization, crystals of the fully reduced enzyme (all ferrous) could only be obtained by anaerobic screening in an anaerobic chamber and in the presence of excess sodium dithionite. Consistent with the behavior of the enzyme in solution, reduced crystals of PfRbr are clear. Oxidation of these crystals could be observed by simply dipping a crystallography tool into an anoxic solution of H_2O_2 and then immediately dipping the same tool into the crystallization well (**Supplemental Movie 2**). Initially, this experiment was performed with wells containing multiple crystals and the diffusion of the peroxide throughout the well was demonstrated by a change in the color of the crystals as they went from clear to red. This can be seen in the Supplemental Movie 2 where a wave of color change begins at the point of addition and extends out through the crystals in the well. It was clear that extensive exposure to peroxide resulted in destruction of the crystals. Therefore, in order to obtain diffraction data we first determined how much exposure to the substrate could be tolerated prior to freezing and loss of diffraction. A significant number of crystals were destroyed prior to accomplishing successful H_2O_2 treatment, freezing and

diffraction and a time course showing the impact on diffraction is included in the supplementary material (**Supplemental Figure 1**). In general, an exposure time between two and ten seconds resulted in diffraction to approximately 2.0Å resolution (Table 1).

Overall structural organization. In contrast to what has been previously reported [25] and what has been observed for the all ferrous iron form or PfRbr (PDB ID 3LU3), our crystals were monoclinic belonging to the space group $P2_1$. Essentially, the treatment of fully reduce PfRbr crystals with the substrate peroxide has resulted in a change in space group symmetry from the high symmetry space group $P4_22_12$ to the lower symmetry space group $P2_1$. However, the shift in space group symmetry does not result in a significant change in the unit cell (a=80 b=105.1 c=105.2 α=90.0 β=90.1 γ=90.0 for $P2_1$ compared with a=105.4 b=105.4 c=80.0 α=90.0 β=90.0 γ=90.00 for $P4_22_12$). Combined with the lower symmetry space group, these observations indicate that there are more copies of the peptide monomer in the asymmetry unit. In fact, eight peptide chains were observed in the asymmetric unit resulting in four domain-swapped monomers per asymmetric unit. As can be seen in Figure 2, each monomer contributes two helices to the domain-swapped hemerythrin domain and also contains a mononuclear iron site in the rubredoxin domain. If all eight of the monomers in the asymmetric unit were structurally identical, then the tetragonal space group ($P4_22_12$) would prevail.

Catalytic intermediates of PfRbr. After model building and refinement it became clear that there were structural differences between the eight individual monomers in the asymmetric unit. These differences account for the change in space group symmetry and are the result of the peroxide treatment and the capture of different catalytic intermediates at the diiron site. These intermediates are presented in Figure 3 and further result in conformational changes contained predominantly within the four-helix bundle. In large part the conformational changes are the

result of the redox-dependent iron movement at the active site. The most populated intermediate appears to be the previously identified mixed-valent species. This intermediate is observed in six of the eight diiron active sites (Figure 3, Panel A). This observation confirms that, like the homologous enzyme from the mesophilic organisms, the thermophilic rubrerythrin also undergoes the redox-dependent iron movement. This catalytic intermediate has been substantially characterized in the mesophilic rubrerythrins (DvRbr and DvNgr) by spectroscopic and structural studies [15-18], but this is the first observation of such a species for any thermophilic rubrerythrin from an archeal organism.

Previous work supports the hypothesis that the oxygen atom in the μ-oxo bridge is derived from the substrate, peroxide [22-24]. Interestingly, if the diiron site in the hemerythrin domain, constructed from monomers F and K, is modeled with a single bridging oxygen atom, then a 3.2 σ peak appears in the difference map (Figure 3 Panel B, green cage) suggesting that the single oxygen atom is insufficient to account for the observed density between the iron atoms. The composite omit map is also consistent with there being additional density at this position and the difference density was only satisfied by modeling this as a peroxy anion (See Figure 3, Panel B). Whether this represents a hydro- or dihydro-peroxy anion is not clear, but what is clear is that the single oxygen of the μ-oxo atom alone does not satisfy the observed electron density. In addition to this observation, further model building revealed another surprising finding. As shown in Figure 3, Panel C, the diiron site found between monomers D and I does not have any bridging μ-oxo atom.

In the currently accepted model for peroxide reduction, the peroxide-derived oxo bridge, in both the di-ferric μ-oxo and mixed-valent μ-hydroxo forms, can readily exchange with an oxygen atom from solvent [22-24]. Since it is known that the Fe(III)-(μ-hydroxo) bonds are

longer than Fe(III)-(μ-oxo) bonds (see Table 2) and Fe(II)-O(solvent) bonds would be weaker than Fe(III)-O(solvent) bonds, the mixed-valent μ-hydroxo should be even more solvent exchangeable. Moreover, for the all-ferric form of the diiron center, reduction by the rubredoxin domain results in the mixed-valent state. Since this internal electron transfer event should occur much faster than the solvent exchange, we therefore propose that the data we observe in Figure 3, Panel C, is most likely due to the loss of the peroxide-derived μ-hydroxo bridge as water. In addition, because the crystals were fully reduced (the diiron and rubredoxin irons are all ferrous) before the peroxide was added and no additional chemical reductant was present during peroxide treatment, we propose that the loss of the peroxide-derived μ-hydroxo oxygen has occurred after internal electron transfer from the rubredoxin domain.

An updated mechanism is depicted in Figure 4 that incorporates these results and previous spectroscopic and structural work performed on DvRbr and DvNgr. Since peroxide has the potential to rapidly obtain two electrons, one from each iron atom, the degradation of the peroxide bound species to a hydro-peroxy would occur rapidly as the iron atom, previously bound to H55, moves away from the histidine nitrogen atom and forms a new bond with E83. Moreover, since the removal of a second electron from the next iron atom in the diiron site would occur almost simultaneously, the rapid release of the first water molecule does not result in any radical formation, but rather a bridging oxygen atom with a complete octet in the di-ferric form (Intermediate 1 in Figure 4).

Destabilization of the alpha helix. As previously mention, PfRbr rapidly precipitates when fully oxidized, a process that is completely reversible. Some insight into the mechanism of the oxidative precipitation is found in the data presented here. As a direct result of oxidation and iron movement, structural changes occur in the helix containing residue E114, which serves as a

bridging ligand to the diiron site (Figure 5). Specifically, the redox-dependent iron movement results in a distortion of this α helix such that the geometry required for optimal hydrogen bonding in an alpha helix is no longer maintained. Specifically, we observe a difference of up to 1.7 Å for the Cα atoms for several residues in this region when the coordinates of the fully reduced and oxidized states are compared (Figure 5). The carboxyl group of the glutamate residue moves only 0.41Å during oxidation, but a significant destabilization of the helix occurs in order for the peptide backbone to accommodate movement of the bridging glutamic acid ligand occurs and this is what leads to the destabilization of the helix through partial unwinding. We propose that this unwinding is what subsequently leads to the oxidative precipitation seen in both the liquid and crystal forms of the protein.

DISCUSSION

Catalytic intermediates in oxygen-oxygen bond cleavage. Capturing intermediates within the active site of metalloenzymes that have high turnover numbers is extremely challenging, but has also provided a wealth of information about how metals in biology are used to catalyze difficult and essential chemical reactions [28-35]. A significant amount of work has focused on metalloenzymes that either activate molecular oxygen or serve to remove reactive oxygen species. Moreover, due to electronic properties of heme and the spectroscopic techniques that can be applied, much of this work has focused on cytochrome containing enzymes. Of particular interest to the data presented here are recent efforts to capture the hydro peroxy anion or oxyferryl (compound I) intermediates in the cytochrome-containing peroxidases and in related model compounds [32, 36, 37]. In contrast to the heme peroxidases, similar attempts to capture turnover intermediates in the diiron peroxidases have not been reported. This is not the case for all non-heme iron enzymes and significant progress has been made for enzymes such as methane

monooxygenase (MMO) or the extradiol dioxygenases [28, 29, 38, 39]. Recent work with the monooxygenase system has shown the existence of multiple intermediates that are involved in oxygen activation and that the conversion is pH dependent [40]. In the extradiol dioxygenase system, work with norcarane and bicyclohexane and the ratio of their unrearranged to rearranged products allowed for estimation of radical lifetimes and it was ultimately shown that the mechanism proceeded by a radical intermediate [41]. A very interesting recount on the discovery of intermediates from these systems using spectroscopic and crystallographic analyses of homoprotocatechuate 2,3-dioxygenase, naphthalene 1,2-dioxygenase, benzoate 1,2-dioxygenase, and methane monooxygenase has been described [29]. However, the latter work presented the first evidence for a peroxy anion (either hydro- or dihydro-peroxy) in any peroxidase system (cytochrome or non-heme iron) albeit for a mono-nuclear iron site that activates molecular oxygen.

A catalytic model for rubrerythrin. Rubrerythrins, and PfRbr in particular, are selective for peroxide reduction and have evolved to avoid high-valent iron intermediates during turnover [2, 7, 11, 13]. The underlying mechanism for selective reduction of peroxide has been proposed to be linked to the redox-dependent iron movement and the geometry of the fully reduced diiron site [13, 16]. These functional observations are somewhat surprising considering that rubrerythrins also contain a pair of EX_{29-32}-EX_2H amino acid sequences that are similar to sequences found in the diiron ezymes that activate molecular oxygen [13, 42, 43]. This includes enzymes such methane monooxygenase and the iron storage enzyme bacterioferritin. In contrast, rubrerythrins do not bind molecular oxygen reversibly nor has the activation of molecular oxygen ever been observed [42, 43]. Rubrerythrins also tend to be much smaller than these O_2-activating enzymes and do not form large oligomers in solution. Moreover, the reduction

potential for the Fe^{3+}/Fe^{2+} couple in both the diiron and $[Fe(Cys)_4]$ sites are also relatively high ($E°'$ > 200 mV vs. NHE) [19, 23] insuring that, especially for a strict anaerobe, these enzymes remain in the all-ferrous state under physiological conditions. Therefore, the rapid simultaneous two-electron reduction of peroxide by rubrerythrins has been the favored model because it also avoids production of a hydroxyl radical that would result from a single electron reduction of peroxide. The observation of intermediate 0 (see Figure 4) suggests that while electron transfer to substrate is indeed rapid, the cleavage of the O-O bond and loss of water still proceeds by a stepwise heterolytic mechanism. This is a significant finding considering that, in the traditional sense, the cleavage of the O-O bond by an Fe(II)- hydroperoxy complex is thought to proceed via homolytic O-O bond cleavage resulting in the production of a hydroxyl radical and an Fe(III)-oxo(OH^-) species [44-46]. The presence of a bridging peroxy intermediate significantly changes the mechanistic view of rubrerythrins and suggests that radical-free heterolytic bond cleavage is achieved in part through a bridging peroxy complex and rapid transfer of another electron from the second Fe(II) atom followed by release of water and formation of the all-ferric diiron species (labeled as intermediate I in Figure 4). In this case, the mechanism would suggest that the *simultaneous* two electron reduction of peroxide does not occur. This adds an important new facet to our understanding of the mechanism of rubrerythrins and further underscores the importance of the redox-dependent iron toggling observed for these enzymes. The active site geometry of the ferrous diiron center is optimized for peroxide, not molecular oxygen binding, and the redox toggling insures that superficial oxidation of the diiron site results in iron movement, further decreasing the reactivity of the active site towards oxygen. Moreover, because *P. furiosus* represents an evolutionarily old organism, this appears to be a mechanistic feature of rubrerythrins that Nature identified early. The mechanism outline in Figure 4 also

implies that in the absence of an external electron source that could re-reduce the rubredoxin iron site, the loss of the second peroxide-derived oxygen atom can still occur. This conclusion is based on the fact that our experiment began with PfRbr in an all ferrous state with a total of three ferrous iron atoms (two in the diiron site and one in the rubredoxin domain). Crystals were then dropped into anaerobic mother liquor containing peroxide and no additional reductant. Therefore, after peroxide treatment and reduction each diiron site can only be reduced by the single electron remaining in the ferrous iron of the rubredoxin domain. In theory, the diiron site would be left in the mixed-valent state and even though we have proposed that the active site lacking a μ-oxo bridge is the result of the loss of water from the mixed-valent state (See Figure 4), we can not confirm the oxidation state of the iron atoms at this time. It will be interesting to investigate whether or not the experiment can be performed at lower temperatures to further slow the reactivity of the enzyme and increase the population of the peroxy intermediate. Likewise, if additional reductant were present of if the population of the peroxy intermediate can be increased, we would predict that an active site lacking a μ-oxo bridge will not be observed.

Redox-dependent changes in enzyme solubility. Another interesting observation seen in the data reported herein is the destabilization of the helix containing E114 upon oxidation of the diiron site. The peptide bond geometry at this point is such that it does not meet the requirements needed in order to maintain the helical structure. This observation is consistent with previous calculations of forces on the equivalent residue in the structure of methane monooxygenase from *Methylococcus capsulatus* [47]. The monooxygenase structure is similar to that of rubrerythrin in that it is composed of a four-helix bundle with four acidic residues as well as the two histidine ligands coordinating the diiron site but there is one more glutamic acid residue involved in the coordination of the iron atoms in the active site of rubrerythrin. The

peptide from methane monooxygenase has been hypothesized to play a major role in catalysis, by differentially compressing the diiron distance for the various states of the active site during the catalytic cycle [47]. These calculations show that equivalent glutamic acid residue of methane monooxygenase exerts the greatest force on the diiron site out of all of the glutamate residues involved in the active site. The equivalent residue in the structure described herein is the site of the unwinding of the helix, which is in accord with the calculations of forces placed upon the same residue in the monooxygenase during catalysis.

In general, the redox toggling of the iron atom at the Fe^{2+}/Fe^{3+} couple combined with the immediate availability of two additional electrons, one from the second ferrous iron in the diiron site and another from the ferrous iron of the rubredoxin domain, can account for the peroxide selectivity over oxygen and the rapid two electron reduction of peroxide. The fact that the all-ferric form of the enzyme precipitates and the observations presented in this work that the redox toggling occurs in PfRbr has several important implications. First, this suggests that *in vivo* the reduction of the rubredoxin domain of PfRbr by cytoplasmic rubredoxin occurs very quickly in order to avoid precipitation. Second, this work also implies that the structural features that account for peroxide selectivity over molecular oxygen were adopted by the rubrerythrin family very early on an evolutionary scale after this toxic species became available.

METHODS

Enzyme expression, isolation, and crystallization. Rubrerythrin was purified as previously described except that 30g of cells were broken and the protocol was adjusted for the larger amount of protein present and all manipulations were carried out under strictly anaerobic conditions [11]. Purity was checked by SDS-PAGE analysis and the protein was concentrated to 15.6 mg/ml and screened using the robot at 0.5µl of protein to 0.5µl of crystallization condition.

All plates were covered with 4ml of 80:20 paraffin oil:silicon oil. The protein crystallized after eight days in 0.1M Bis-Tris pH 6.5 and 28% w/v polyethylene glycol monomethyl ether 2,000 in an anaerobic chamber in modified microbatch. A single crystal was harvested with a cryoloop (Hampton Research, HR4-747) and briefly immersed in a 1 µl drop containing a 1:4 mixture of glycerol and the precipitant solution. Once the crystal was placed in the cryoprotectant, H_2O_2 was added by touching a concentrated stock with a crystal manipulation tool and then touching that to the 1µl drop. The crystal then turned red due to oxidation of the iron atoms and was then immediately frozen and stored in liquid nitrogen. It was very important to freeze the crystal as quickly as possible after oxidation as prolonged exposure to oxidative conditions ruined the diffraction quality (**see Supplemental Figure 1**). Unless otherwise stated all manipulations were carried out in an anaerobic chamber where oxygen levels were maintained below 1 ppm.

Data collection and processing. Data were collected at 22-BM Advanced Photon Source, Argonne National Laboratory using a MAR 225 charge-coupled device (CCD) detector with 1 second exposures of 0.97Å X-rays. 360° worth of data was collected at 1° intervals. During data collection, the crystal turned from dark red to a pinkish color, but not to the clear form seen in the reduced state of the protein or previously reported for DvRbr and DvNgr. The data was collected, integrated and scaled using HKL2000 [48]. Molecular replacement was carried out using the 2HR5 from the protein data bank and the program PHASER from the CCP4 program suite [49]. Multiple cycles of model building in COOT followed by refinement with Refmac from the CCP4 program suite completed the structure solution with R_{work} = 22.4 % and R_{free} = 27.4 % [50]. The model and structure factors for the peroxide-treated PfRbr crystal has been deposited under the PDB ID code 3MPS.

ACKNOWLEDGEMENTS

This research was supported by NSF grant MCB 0835432 to W.N.L. and a grant (DE-FG05-95ER20175) from the Chemical Sciences, Geosciences and Biosciences Division, Office of Basic Energy Sciences, Office of Science, U.S. Department of Energy.

Table 4.1, Data collection and refinement statistics[a].

X-ray Source	APS22BM
Detector	MAR225 CCD
Wavelength (Å)	0.97
Oscillation Width (°)	1.0
Number of frames	360
Resolution (Å)	47.0-2.0 (2.07-2.0)[b]
Unit Cell Parameters	α=90.1,β=γ=90°
a ≠ b ≠ c (Å)	80.4, 105.16, 105.22
Space Group	$P2_1$
Redundancy	7
Unique reflections	12,220
Completeness	99.8(97.9)
I/Sigma(I)	19.3(2.8)
Rsym	12.1(37.3)[c]
R_{cryst} (%)	22.4
R_{free} (%)	27.4
RMSD bonds (Å)	0.022
RMSD angles (°)	1.781
Average B factor	24.7

[a]A 360 º data set was collected at 1.0 Å on a single Rbr crystal that had been prepared under anaerobic and reducing conditions before being exposed to anaerobic mother liquor containing H_2O_2 as described in the Materials and Methods. [b]Numbers in parenthesis correspond to the data in the outermost resolution shell. [c] $R_{sym} = \sum_{hkl}[\sum_I(|I_{hkl,I} - \langle I_{hkl}\rangle|)]/\sum_{hkl,I}\langle I_{hkl}\rangle$, where I_{hkl} is the intensity of an individual measurement of the reflection with indices hkl and $\langle I_{hkl}\rangle$ is the mean intensity of that reflection.

Table 4.2. Interatomic distances for metal sites in the crystal structures of the PfRbr, DvRbr, and DvNgr.

Atoms[a]	Oxo-bridged	Peroxide Bound	No oxo-bridge	Reduced	DvNgr(120 [b])[c]	DvNgr(360 [d])[c]	$DvNgr_{red}$ [ce]	$DvRbr_{ox}$ [e,f]	$DvRbr_{red}$ [e,f]
Fe1-E114(B)OE2/128/149	2.0	2.0	2.0	2.0	2.0	2.0	2.0	2.0	2.1
Fe1-E52(A)OE1/53/73	2.0	2.0	2.0	2.1	2.2	2.2	2.1	2.2	2.1
Fe1-E83(B)OE1/97/118	2.0	2.0	2.0	4.3	2.2	2.1	4.1	2.1	4.6
Fe1-E19(A) OE1/20/40	2.4	2.1	2.4	2.5	2.1	2.1	2.2	2.1	2.2
Fe1-E19(A) OE2/20/40	2.1	2.1	2.0	2.0	2.3	2.3	2.3	2.3	2.3
Fe1-E52(A)OE2/53/73	2.1	2.1	2.1	2.1	2.0	2.0	2.0	2.0	2.1
Fe1-H55(A)ND1/56/76	4.3	4.1	4.2	2.3	4.0	4.0	2.2	4.2	2.3
Fe1-O(oxo/peroxide/water)	2.0	2.1	n/a	3.1	2.0	2.0	2.3	1.8	2.2
Fe2-E80(B)OE1/94/115	2.1	2.1	2.1	2.3	2.2	2.2	2.2	2.2	2.2
Fe2-E80(B)OE2/94/115	2.1	2.0	2.1	2.3	2.3	2.3	2.3	2.2	2.3
Fe2-E114(B)OE1/128/149	2.1	2.0	2.0	2.1	2.0	2.0	2.1	2.1	2.1
Fe2-H117(B)ND1/131/152	2.0	2.5	1.9	2.2	2.2	2.2	2.2	2.2	2.2
Fe2-O(oxo/peroxide/water)	2.0	2.0	n/a	2.2	2.2	2.3	2.2	2.1	2.2
Fe1-Fe2	3.5	3.3	3.3	3.8	3.4	3.4	4.0	3.3	4.0
Fe1-Fe3[g]	14.6	14.7	14.7	13.9	14.3	14.4	12.8	12.4	11.0
Fe2-Fe3[g]	14.3	14.3	14.3	12.8	13.0	13.1	13.2	12.0	12.2

[a]For amino acid residues, the first identifier is for pfRbr the second number listed after the (/) is for DvRbr and the third is for the equivalent DvNgr residue (Data from Jin et al.). [b]Frames 1-120 of data collected on oxidized DvNgr crystal at 0.98-Å X-ray wavelength (Data from Iyer et al.). [c]Distances are averages for monomers A and B in data from Iyer et al. Distances for the alternate "reduced" Fe1 position (cf. text and Fig. 4c) are not included. [e]Subscripts "ox" and "red" indicate all-ferric and all-ferrous, respectively.

Figure 4.1. Proposed mechanistic scheme for peroxidase (hydrogen peroxide reductase) activity of Rubrerythrin (adapted from [13]). Glutamate ligands other than the glutamate side chain involved in redox toggling of the iron have been omitted for clarity. The toggling iron is shown in red and the oxygen atoms originating from peroxide are filled in black.

Figure 4.1, Dillard et al.

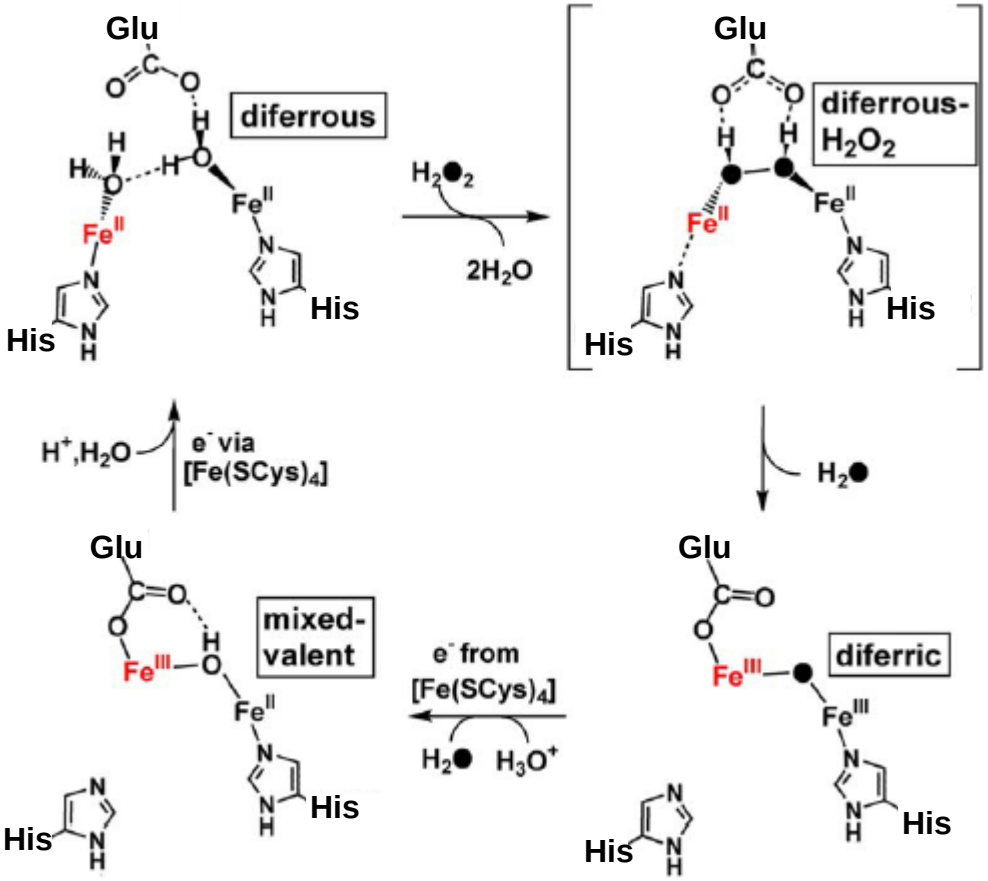

Figure 4.2. Overall topology of the asymmetric unit in H_2O_2 treated crystals of reduced rubrerythrin from *P. furiosus*. Cartoon representation of the secondary structure with each monomer in the asymmetric unit colored uniquely and the iron atoms represented by black spheres. The asymmetric unit contains eight monomers that comprise four domain-swapped dimers. Panel A is identical to Panel B after a 90 ° rotation about the X-axis.Figure 4.2, Dillard et al.

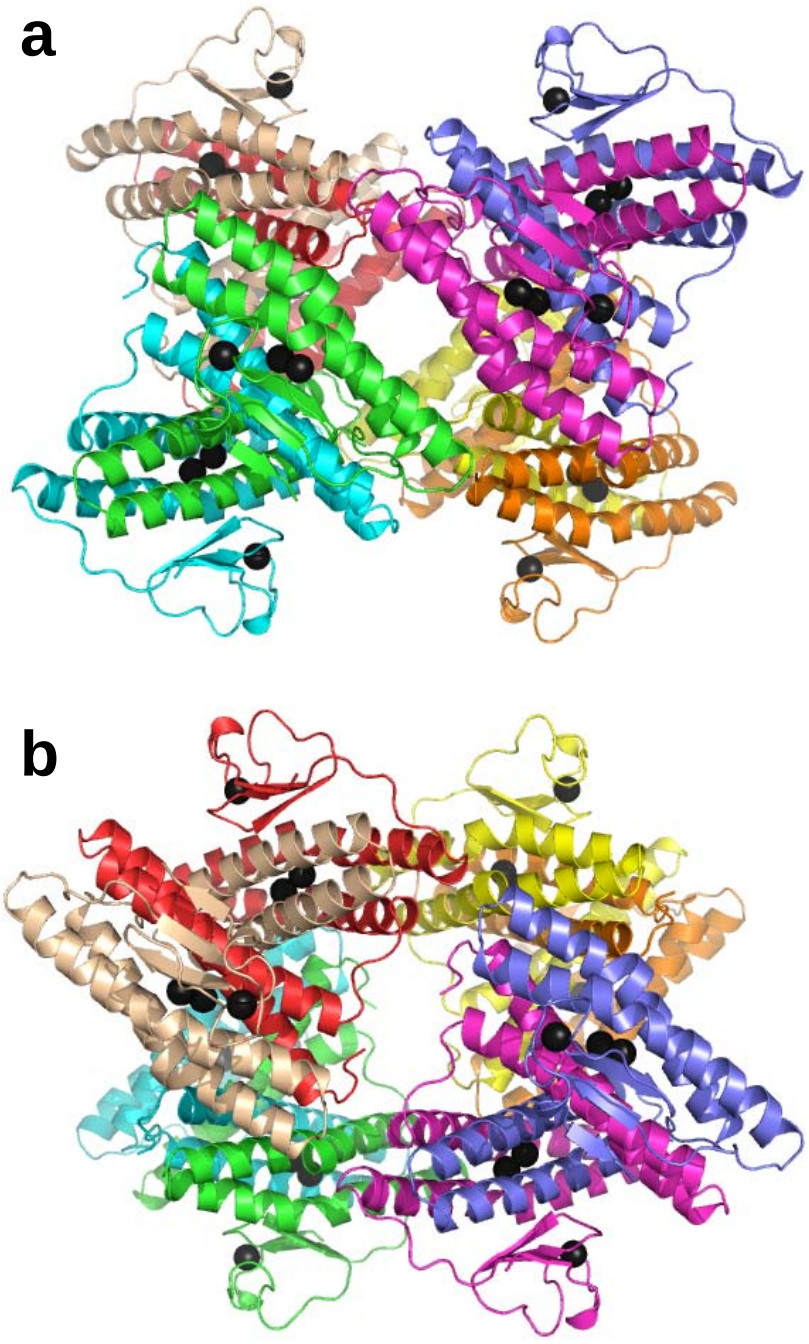
a
b

Figure 4.3. Wall-eyed stereo view of the models and electron density for the diiron active sites in the domain-swapped dimer composed of monomers A & B (*Panel A*), monomers F & K (*Panel B*), and monomers G & H (*Panel C*). The $2Fo\text{-}F_c$ composite omit map (blue cage) was generated using the simulated annealing protocol with 7% of the model omitted per cycle and is contoured at one sigma. The difference map ($F_o\text{-}F_c$) shown in Panel B (green cage) was generated after omission of the peroxide molecule and a single oxy atom is modeled bridging the iron atoms. The resulting difference map shown in the Panel B is contoured at 3.2 sigma.Figure 4.3, Dillard et al.

a

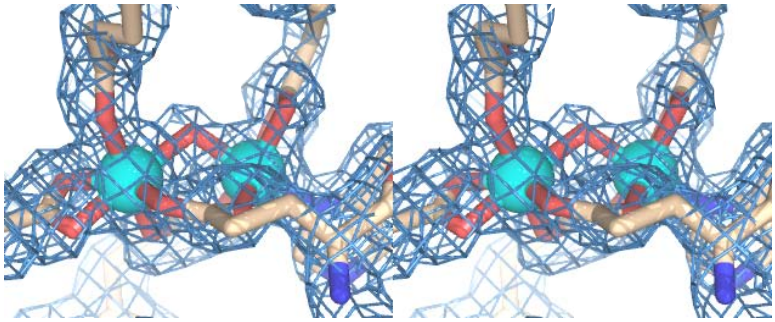

b

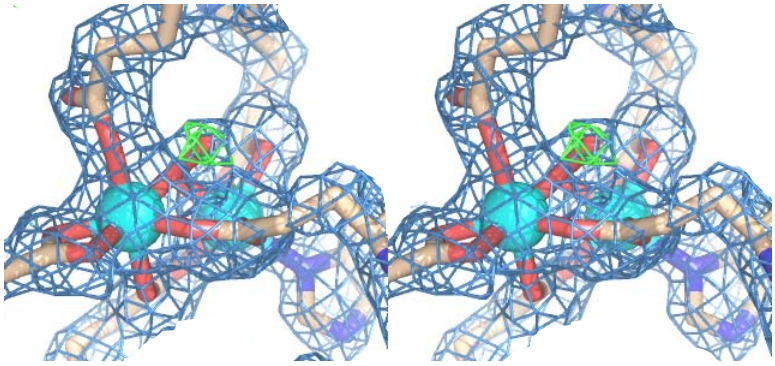

c

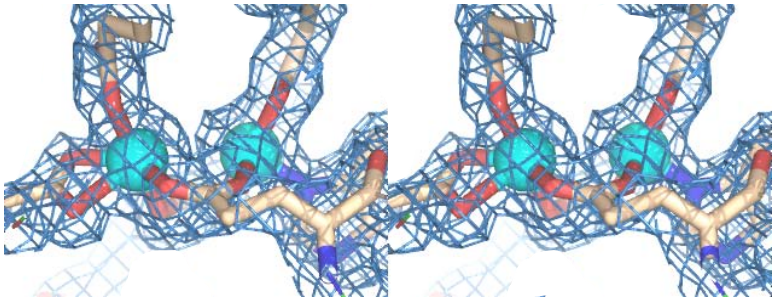

Figure 4.4. Mechanistic scheme for peroxidase (hydrogen peroxide reductase) activity of PfRbr. The glutamate ligand is that of E83 all others are omitted for clarity. This glutamate residue is a strictly conserved residue in all rubrerythrins. Similarly, H55 and H117 are also conserved residues with His 55 being a ligand to the toggling iron atom in PfRbr during turnover. Oxygen atoms that are derived from peroxide are shown in bold lettering.Figure 4.4, Dillard et al.

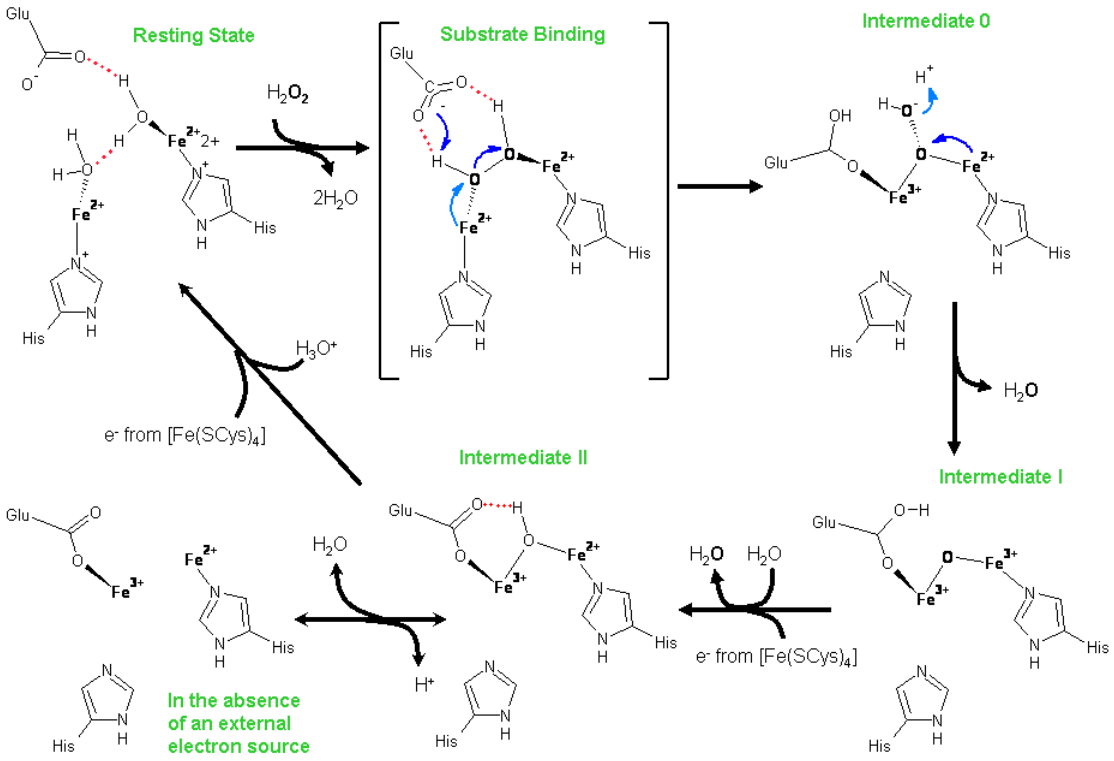
Resting State
Substrate Binding
Intermediate 0
Intermediate I
Intermediate II
H_2O_2
$2H_2O$
H_3O^+
e- from $[Fe(SCys)_4]$
H_2O
H^+
In the absence of an external electron source

Figure 4.5. Redox-dependent changes that are proposed to influence enzyme solubility. Movement of E114 upon oxidation of the all ferrous diiron center (Purple Model) to the fully oxidized all ferric state (Green Model) results in a significant distortion of an α helix. The movement of backbone carbon atoms is over 1.7 angstroms in some cases. The helix is shown as a cartoon while the metal ligands are labeled and represented by the stick models.

Figure 4.5, Dillard et al.

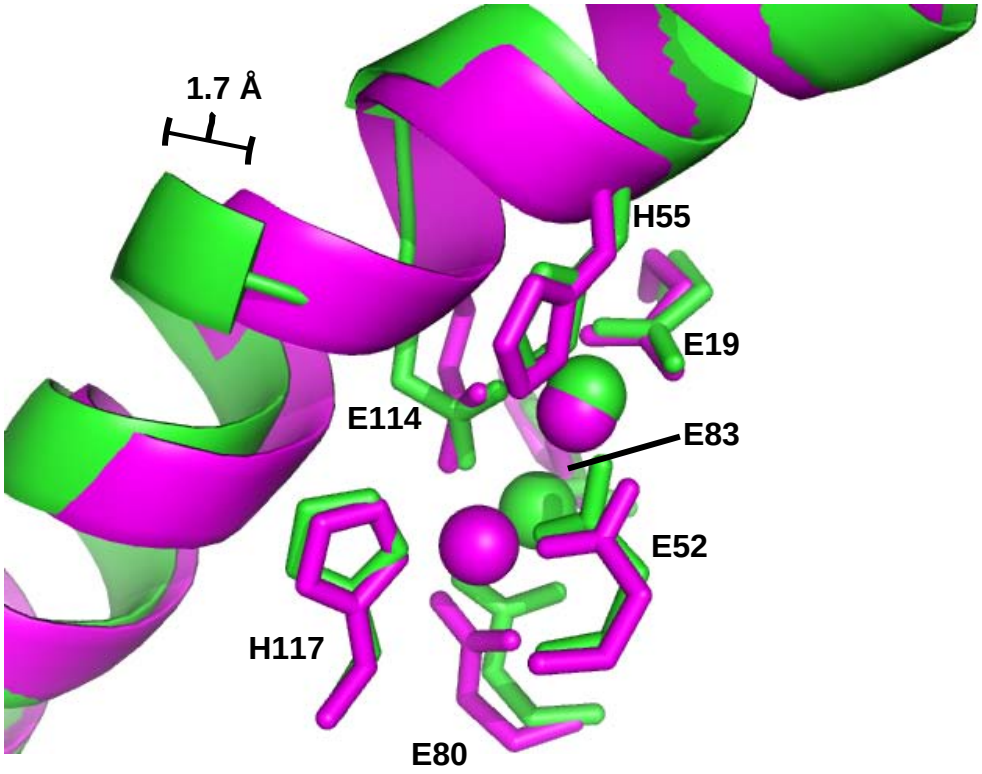

REFERENCES

1. Massey, V., et al., *Biochemical and Biophysical Research Communications,* 1969. **36**(6): p. 891-&.
2. Riebe, O., et al., *Microbiology,* 2009. **155**(Pt 1): p. 16-24.
3. Imlay, J.A., *Adv Microb Physiol*, 2002. **46**: p. 111-53.
4. Imlay, J.A., *J Biol Inorg Chem*, 2002. **7**(6): p. 659-63.
5. Lumppio, H.L., et al., *J Bacteriol*, 2001. **183**(1): p. 101-8.
6. Jenney, F.E., Jr., et al., *Science*, 1999. **286**(5438): p. 306-9.
7. Coulter, E.D. and D.M. Kurtz, Jr., *Arch Biochem Biophys*, 2001. **394**(1): p. 76-86.
8. Coulter, E.D., N.V. Shenvi, and D.M. Kurtz, Jr., *Biochem Biophys Res Commun*, 1999. **255**(2): p. 317-23.
9. Sztukowska, M., et al., *Mol Microbiol*, 2002. **44**(2): p. 479-88.
10. Alban, P.S., et al., *J Appl Microbiol*, 1998. **85**(5): p. 875-82.
11. Weinberg, M.V., et al., *J Bacteriol*, 2004. **186**(23): p. 7888-95.
12. May, A., et al., *FEMS Microbiol Lett*, 2004. **238**(1): p. 249-54.
13. Kurtz, D.M., Jr., *J Inorg Biochem*, 2006. **100**(4): p. 679-93.
14. deMare, F., D.M. Kurtz, Jr., and P. Nordlund, *Nat Struct Biol*, 1996. **3**(6): p. 539-46.
15. Jin, S., et al., *J Am Chem Soc*, 2002. **124**(33): p. 9845-55.
16. Iyer, R.B., et al., *J Biol Inorg Chem*, 2005. **10**(4): p. 407-16.
17. Jin, S., et al., *J Inorg Biochem*, 2004. **98**(5): p. 786-96.
18. Jin, S., et al., *Biochemistry*, 2004. **43**(11): p. 3204-13.
19. Pierik, A.J., et al., *Eur J Biochem*, 1993. **212**(1): p. 237-45.
20. Lumppio, H.L., et al., *J Bacteriol*, 1997. **179**(14): p. 4607-15.
21. Bonomi, F., D.M. Kurtz, Jr., and X. Cui, *J. Biol. Inorg. Chem.*, 1996. **1**(1): p. 67-72.
22. Dave, B.C., et al., *Biochemistry*, 1994. **33**(12): p. 3572-6.
23. Gupta, N., et al., *Biochemistry*, 1995. **34**(10): p. 3310-8.
24. Smoukov, S.K., et al., *Biochemistry*, 2003. **42**(20): p. 6201-8.
25. Tempel, W., et al., *Proteins*, 2004. **57**(4): p. 878-82.
26. Fushinobu, S., H. Shoun, and T. Wakagi, *Biochemistry*, 2003. **42**(40): p. 11707-15.
27. Wakagi, T., *FEMS Microbiol Lett*, 2003. **222**(1): p. 33-7.
28. Kovaleva, E.G. and J.D. Lipscomb, *Science*, 2007. **316**(5823): p. 453-7.
29. Kovaleva, E.G., et al., *Acc Chem Res*, 2007. **40**(7): p. 475-83.
30. Poulos, T.L., *Philos Transact A Math Phys Eng Sci*, 2005. **363**(1829): p. 793-806; discussion 1035-40.
31. Sligar, S.G., T.M. Makris, and I.G. Denisov, *Biochem Biophys Res Commun*, 2005. **338**(1): p. 346-54.
32. Meharenna, Y.T., et al., *Biochemistry*, 2010. **49**(14): p. 2984-2986.
33. Hersleth, H.P., et al., *J Biol Chem*, 2007. **282**(32): p. 23372-86.
34. Berglund, G.I., et al., *Nature*, 2002. **417**(6887): p. 463-8.
35. Nakamura, T., et al., *Proc Natl Acad Sci U S A*, 2008. **105**(17): p. 6238-42.
36. Karlin, K.D., *Nature*. **463**(7278): p. 168-9.
37. Liu, J.G., et al., *Angew Chem Int Ed Engl*, 2009. **48**(49): p. 9262-7.
38. Bailey, L.J. and B.G. Fox, *Biochemistry*, 2009. **48**(38): p. 8932-9.
39. Sazinsky, M.H., et al., *Biochemistry*, 2006. **45**(51): p. 15392-404.
40. Tinberg, C.E. and S.J. Lippard, *Biochemistry*, 2009. **48**(51): p. 12145-58.

41. Chakrabarty, S., et al., *J Am Chem Soc*, 2007. **129**(12): p. 3514-5.
42. Kurtz, D.M., Jr. and B.C. Prickril, *Biochem Biophys Res Commun*, 1991. **181**(1): p. 337-41.
43. Kurtz, D.M., Jr., *J. Biol. Inorg. Chem.*, 1997. **2**(2): p. 159-167.
44. Haber, F. and J. Weiss, *Proc. R. Soc. London, Ser. A*, 1934. **147**(332-351).
45. MacFaul, P.A., D.D. Wayner, and K.U. Ingold, *Acc Chem Res*, 1998. **31**: p. 159-162.
46. Walling, C., *Acc Chem Res*, 1975. **8**: p. 125-131.
47. Rinaldo, D., et al., *J Am Chem Soc*, 2007. **129**(11): p. 3135-47.
48. Otwinowski Z, M.W., *Methods Enzymol* (1997)(A276): p. 307-326.
49. *Acta Crystallogr D Biol Crystallogr*, 1994. **50**(Pt 5): p. 760-3.
50. Murshudov, G.N., A.A. Vagin, and E.J. Dodson, *Acta Crystallogr D Biol Crystallogr*, 1997. **53**(Pt 3): p. 240-55.

CHAPTER 5

DISCUSSION

In the previous chapters it has been shown that different metal centers in different proteins, when maintained in an anoxic environment, allow two distinct enzymes to carry out their biological functions. The enzyme discussed in chapter 2, proline dehydrogenase 1, was shown to contain a [2Fe-2S] cluster that is involved in electron transfer from proline. The possibility that this enzyme could contain a cluster had been tested previously, but for unknown reasons the authors of that work were unable to detect it (*1*). This enzyme has been quite elusive in its characterization in that the crystal structure of the enzyme showed residues that are conserved in related amine dehydrogenases that could be involved in catalysis. Upon mutation of the three residues, the enzyme maintained its native activity showing that they are not involved in the catalytic mechanism (*1*). Although in chapter 2 it was shown that the cluster exists, the physiological electron acceptor is still unknown for this enzyme. Acceptors such as NAD^+, $NADP^+$, ferredoxin, and rubredoxin from *P. furiosus* were tested but none showed any activity. Perhaps the native enzymatic activity is a bifurcating system and this possibility was tested as well using different combinations of NAD(H), NADP(H), and *P. furiosus* ferredoxin but yet again no activity was detected. The bifurcating system has previously been shown to exist in archaea and could still be used by this particular enzyme but the right combination of donors and acceptors was not discovered during the course of this work (*2*). This system exists in methanogenic archaea that do not contain cytochromes as part of their respiratory system. The

enzymes responsible for bifurcation have a similar flavin composition as that seen in proline dehydrogenase 1 from *P. furiosus* and the closely related *P. horikoshii* (*1-3*).

There are still many unanswered questions concerning *P. furiosus* PDH1 and the answers should be quite intriguing. Questions include, do the four cysteine residues seen in the x-ray crystal structure coordinate the cluster, which residues are responsible for catalyzing oxidation of proline, is it a bifurcating system, does the ATP molecule seen in the x-ray crystal structure play a role in activity, and what is the electron acceptor for the enzyme?

In chapters 3 and 4 the enzyme rubrerythrin was investigated by x-ray crystallography. Much of the work done previously on this enzyme has been carried out with the rubrerythrin form the mesophilic bacterium *Desulfovibrio vulgaris* (*4-17*). The enzyme from *D. vulgaris* was shown to coordinate multiple metals in its three metal binding sites and the enzyme would have different activities depending upon which metal was present. The activities attributed to this enzyme are ferroxidase, peroxidase, and pyrophosphatase (*12, 18-20*). A catalytic mechanism was proposed from a series of x-ray crystal structures solved in different redox states of the enzyme and with a substrate mimic for hydrogen peroxide (*7*).

Rubrerythrin from *P. furiosus* has also been well characterized and has been shown to also coordinate different metals in its three metal binding sites, but only when the enzyme coordinates iron in all three sites is activity detectable (*21, 22*). That activity is hydrogen peroxide reduction and this enzyme is included in the system required for removal of reactive oxygen species from the organism (*22*). A unique feature of this enzyme is that when it is exposed to oxygen or to an excess of oxidant it becomes insoluble. This is not the case for the enzyme from *D. vulgaris.* In addition, while the enzyme from *P. furiosus* has its highest activity at or above 90 °C, it retains three percent of its activity at 23°C. While the mesophilic

counterpart may also have three percent of its activity at -50°C (~80°C below the optimum growth temperature of the organism) it is not readily measureable. The differences between the two enzymes lead to the crystallographic work described in chapters 2 and 3.

The merging of the Douglas Instruments crystallization robot with the anaerobic chamber was essential in determining the x-ray crystal structure of rubrerythrin and consequently the mechanism that was elucidated from the trapped peroxy-anion intermediate. The trapping of the intermediate was only possible because we were carrying out "cryo-enzymology" at room temperature of a protein from *P. furiosus*, a hyperthermophile. In other words, we were working ~80°C below the temperature optimum of the organism. The fact that the space group was $P2_1$ and not $P4_22_12$ as in the reduced form was quite helpful in the determination of the mechanism. It allowed for eight distinct active sites to be constructed into the electron density and displayed three different active site states where one had no oxo-bridge, another had the anion bound, and the other six contained the typical oxidized oxo-bridge form. The mechanism proposed for the enzyme from *D. vulgaris* suggested that both electrons from the two iron atoms were transferred in a concerted manner but the existence of the peroxy-anion in the structure of the oxidized *P. furiosus* protein removes that possibility.

The trapping of the intermediate described in this work is the first in any peroxidase, be it from a diiron or cytochrome system. There are many other enzymes that use iron as a means to control electron flow in conjunction with oxygen and its various intermediates (*15, 22-25*). Many of the intermediates in these systems have been trapped due to the fact that they use co-substrates. In the mononuclear non-heme oxygen-activating enzymes that function as extradiol aromatic ring cleaving dioxygenases and the [2Fe-2S] Rieske cis-dihydrodiol forming dioxygenases, some intermediates have been trapped and characterized using spectroscopy and

crystallography in anaerobic environments (*24*). In these two systems the activity of each enzyme is thought to be dependent on the availability of oxygen, and minimizing that concentration allowed for the elucidation of the mechanisms involved (*24*). These types of systems in an anaerobic environment enable one co-substrate to be trapped, and then brief exposure to oxygen and very low temperatures leads to the other intermediates being elucidated. This is not the case for the peroxidases such as rubrerythrin.

In the heme peroxidases, most of our understanding of the catalytic cycle stems from EPR experiments that show that one of the two oxygen atoms of the substrate is involved in a Fe^{IV}-oxo bridge (*26*). This work in conjunction with other EPR experiments on the fully reduced and oxidized states of the enzyme led to a mechanism that involves two heme groups with the two different iron atoms going from Fe^{II} to Fe^{III} and Fe^{II} to Fe^{IV} states. There is no evidence that the diiron peroxidase ever reaches an Fe^{IV} state and there has recently been a review discussing how the enzyme is engineered by Nature to avoid that state (*25*).

The work described in this dissertation has added to the understanding of how the enzyme proline dehydrogenase 1 transfers electrons through its cofactors and elucidated a new mechanism for hydrogen peroxide reduction in the anaerobic organism *P. furiosus*. In all experiments, anaerobic enzymology and the role of iron have been key elements.

References

1. P. J. Monaghan, D. Leys, N. S. Scrutton, *FEBS J* **274**, 2070 (Apr, 2007).
2. R. K. Thauer, A. K. Kaster, H. Seedorf, W. Buckel, R. Hedderich, *Nat Rev Microbiol* **6**, 579 (Aug, 2008).
3. H. Tsuge *et al.*, *J Biol Chem* **280**, 31045 (Sep 2, 2005).
4. R. C. Coleman, *Biophys J* **96**, 584a (February 2009, 2009).
5. N. Gupta *et al.*, *Biochemistry* **34**, 3310 (Mar 14, 1995).
6. R. B. Iyer, R. Silaghi-Dumitrescu, D. M. Kurtz, Jr., W. N. Lanzilotta, *J Biol Inorg Chem* **10**, 407 (Jun, 2005).
7. S. Jin, D. M. Kurtz, Jr., Z. J. Liu, J. Rose, B. C. Wang, *J Am Chem Soc* **124**, 9845 (Aug 21, 2002).
8. S. Jin, D. M. Kurtz, Jr., Z. J. Liu, J. Rose, B. C. Wang, *J Inorg Biochem* **98**, 786 (May, 2004).
9. S. Jin, D. M. Kurtz, Jr., Z. J. Liu, J. Rose, B. C. Wang, *Biochemistry* **43**, 3204 (Mar 23, 2004).
10. D. M. Kurtz, Jr., B. C. Prickril, *Biochem Biophys Res Commun* **181**, 337 (Nov 27, 1991).
11. J. LeGall *et al.*, *Biochemistry* **27**, 1636 (Mar 8, 1988).
12. M. Y. Liu, J. Le Gall, *Biochem Biophys Res Commun* **171**, 313 (Aug 31, 1990).
13. H. L. Lumppio, N. V. Shenvi, R. P. Garg, A. O. Summers, D. M. Kurtz, Jr., *J Bacteriol* **179**, 4607 (Jul, 1997).
14. H. L. Lumppio, N. V. Shenvi, A. O. Summers, G. Voordouw, D. M. Kurtz, Jr., *J Bacteriol* **183**, 101 (Jan, 2001).
15. A. J. Pierik, R. B. Wolbert, G. L. Portier, M. F. Verhagen, W. R. Hagen, *Eur J Biochem* **212**, 237 (Feb 15, 1993).
16. S. K. Smoukov *et al.*, *Biochemistry* **42**, 6201 (May 27, 2003).
17. J. J. Van Beeumen, G. Van Driessche, M. Y. Liu, J. LeGall, *J Biol Chem* **266**, 20645 (Nov 5, 1991).
18. F. Bonomi, D. M. Kurtz, X. Y. Cui, *Journal of Biological Inorganic Chemistry* **1**, 67 (Feb, 1996).
19. E. D. Coulter, D. M. Kurtz, Jr., *Arch Biochem Biophys* **394**, 76 (Oct 1, 2001).
20. E. D. Coulter, N. V. Shenvi, D. M. Kurtz, Jr., *Biochem Biophys Res Commun* **255**, 317 (Feb 16, 1999).
21. W. Tempel *et al.*, *Proteins* **57**, 878 (Dec 1, 2004).
22. M. V. Weinberg, F. E. Jenney, Jr., X. Cui, M. W. Adams, *J Bacteriol* **186**, 7888 (Dec, 2004).
23. S. Chakrabarty, R. N. Austin, D. Deng, J. T. Groves, J. D. Lipscomb, *J Am Chem Soc* **129**, 3514 (Mar 28, 2007).
24. E. G. Kovaleva, M. B. Neibergall, S. Chakrabarty, J. D. Lipscomb, *Acc Chem Res* **40**, 475 (Jul, 2007).
25. D. M. Kurtz, Jr., *J Inorg Biochem* **100**, 679 (Apr, 2006).
26. N. Ellfolk, M. Ronnberg, R. Aasa, L. E. Andreasson, T. Vanngard, *Biochim Biophys Acta* **743**, 23 (Feb 28, 1983).